JPRS-JST-93-020
24 June 1993

JPRS Report

Science & Technology

Japan

Symposium on Ultra-High Temperature Materials '92

Science & Technology

Japan

Symposium on Ultra-High Temperature Materials '92

JPRS-JST-93-020 *24 June 1993*

CONTENTS

[Selected papers from the Symposium on Ultra-High Temperature Materials '92—Steps to Practical Application of Advanced Materials—held 3-4 December 1992 in Tajimi, Gifu Prefecture, sponsored by Gifu Prefecture, Tajimi City, JUTEM, and JUTEMI]

Symposium on Ultra-High Temperature Materials 1992

Foreword

936C1023A Tajimi CHO KO ON ZAIRYO SYMPOSIUM '92 in Japanese 3 Dec 92 pp 2-3

[English translation of foreword by Gifu Prefectural Government, Tajimi City Office, Chubu Economic Federation, Japan Ultra-High Temperature Materials Research Center, Ltd., and Japan Ultra-High Temperature Materials Research Institute, Ltd., provided by source]

[Text] The development of ultra-high temperature materials is expected in various technical areas, such as aerospace, energy, transportation, and the manufacturing and processing of materials, and its wide applications will be extended to all industries.

With this background, in an effort to become a base for cooperative research involving private industry, academia and the government, the Japan Ultra-Tech Temperature Materials Research Center, Ltd., and the Research Institute, Ltd., have been provided with equipment for the production and evaluation of materials which will exhibit superior strength and functioning under an ultra-high temperature environment of about 2,000°C.

Under these circumstances, and following last December's conference, "The Symposium on Ultra-High Temperature Materials—Steps for the Practical Application of Advanced Materials" is being held in Tajimi. With noted researchers of the advanced materials area having been invited, the symposium is being held to promote materials development and applications. We will welcome the participants to the Japan Ultra-High Temperature Materials Research Center (JUTEM)'s Gifu Center to see the facilities and equipment.

JUTEM is situated at the central part of the eastern hill region of Tajimi City and comprises one of the core facilities of Tono Frontier Science Research Park, which is expected to become an intelligence and communications center open to the world.

The symposium offers an excellent opportunity to better understand ultra-high temperature materials, and we hope it is helpful in the future research and development of advanced materials.

Table of Contents

936C1023B Tajimi CHO KO ON ZAIRYO SYMPOSIUM '92 in Japanese 3 Dec 92 pp 4-7

[English translation of Table of Contents provided by source]

Material Science Experiments Under Space Environment, Development of Japanese Experimental Module (JEM)

936C1023C Tajimi CHO KO ON ZAIRYO SYMPOSIUM '92 in Japanese 3 Dec 92 pp 12-25

[Article by Tadashi Matsushita, Space Station Group, National Space Development Agency of Japan (NASDA); English abstract provided by source]

[Text]

[Abstract]

This paper outlines various material science experiments under a space environment, such as microgravity, by utilizing space shuttles as well as small rockets over the past and next few years in Japan, and refers to the current status of developments of the international space station "Freedom" and the JEM, which is one of the components that has been permanently integrated into "Freedom."

Based on many years of experience obtained from the foregoing material science experiments in small rockets and space shuttles, many material science experiments will be carried out during JEM's forthcoming orbital operation to produce various new materials.

1. Introduction

The National Space Development Agency of Japan (NASDA) was established on 1 October 1969 as the central organization for space development in Japan for the purpose of contributing to the promotion of the development and utilization of space. Twenty-three years have passed since then. During this period, NASDA has launched commercial satellites, including communications, broadcasting, meteorological and marine observation satellites, etc., by seven N-I rockets, eight N-II rockets and nine H-I rockets. These satellites are to perform their objectives utilizing positions in space as in the case of, for example, a geostationary satellite in the sky 36,000 km above the earth.

On the other hand, space is a vast field of vacuum, strong radiation and no gravitation (scientifically, microgravity. Since gravity, even though it is not apparent or only weak, does exist, it should be referred to as "weightless" or "microweight." However, both "no gravity" and "microgravity" have been accepted traditionally.). Projects intended to explore the positive utilization of these properties of space are called space environment utilization projects. Among the space environment characteristics, the high vacuum has a drawback in that when an experiment is to be performed by carrying materials into space, it is difficult to obtain a high vacuum due to the discharge of gases from the surface of the experimental apparatus, etc. Moreover, regarding radiation, atomic oxygen, etc., there is a drawback in that a spatially and temporally constant intensity cannot be obtained. Therefore, at present, of the various aspects of the space environment, the no-gravity field is likely to be utilized.

The NASDA projects aimed at no-gravity experimentation began with the materials experiment in 1980 using the small rocket called the TT-500A. Since then, materials experiments utilizing a small rocket (TR-IA) for space experimentation, the space shuttle, etc., have been carried out.

In this article, we will present one aspect of materials experiments utilizing, from the various aspects of the space environment, the no-gravity field, and will also touch upon the space station development situation, the construction of which as a field for performing experiments on space environment utilization, such as the creation of new materials, is scheduled by the end of this century.

2. No-Gravity Environment and Its Characteristics

In the no-gravity field, convection due to temperature differences will not occur (nonconvection), heavy objects will not sink and light objects will not float, i.e., no separation due to weight differences will occur when materials with different specific gravities are mixed (no sinking or buoyancy), and the pressure at any point within a fluid is the same since there is no pressure difference due to height (no static pressure). In addition, because it is possible to achieve the phenomenon of suspending matter in air without using a container (non-contact flotation) (Figure 1 [not reproduced]), the application of these properties will enable phenomena to be elucidated which have been impossible to confirm on the ground, and new materials to be created that cannot be made on the ground.

3. Means and Method for No-Gravity Experiments

Experiments utilizing no gravity were first started during the latter half of the 1960s. The means for the experiments include (1) a drop tower (no- gravity state for several seconds is created for a free-falling experimental apparatus by evacuating the inside of a tower), (2) an aircraft (creating no- gravity state for several seconds within an aircraft in parabolic flight at high altitude), (3) a balloon (creating no-gravity state for several dozen seconds for an experimental apparatus by using a balloon to transport it to an altitude of 10 km and dropping it), (4) a small rocket (creating no-gravity state for several minutes by launching a small rocket of one or two stages and letting the experimental apparatus undergo parabolic flight from an altitude of approximately 100 km), (5) a free flyer, (6) a space shuttle, and (7) a space station.

Since there are trade-offs among the size and weight of the experimental apparatus, the level and duration of the no-gravity state, the cost for the experiment, etc., for each of these means, selection depends on the purpose and nature of the experiment the user has in mind.

4. Materials Experiments Employing Small Rockets

4.1 Summary of Experimental Project

In the following we will present a partial summary and the results of an experiment employing a small rocket (TR-IA) for space experimentation which was launched successfully on 16 September 1991. TR-IA No 2 was launched on 18 August 1992 for an experiment that was completed successfully. The data obtained is currently being analyzed. In addition, TR-IA No 3 is scheduled to be launched during the summer of 1993.

The TR-IA rocket is a one-stage solid propellant rocket with a total length of approximately 13 meters used to launch a payload including an experimental apparatus of 750 kg to an altitude of approximately 280 km, maintaining a microweight environment of less than 10^{-4} g for more than 6 minutes. After completion of the experiment, the payload is recovered from the sea (Figure 2 [not reproduced]).

Table 1 shows the topics of the small rocket microgravity experiments and the names of cooperating researchers. Figure 3 [not reproduced] presents the experimental apparatus loading situation of the TR-IA No 1.

Table 1. Topics and Collaborators of Microgravity Experiments Using Small Rockets

Experimental Apparatus	Rocket No 1 (16 Sep 91)	Rocket No 2 (18 Aug 92)	Rocket No 3 (Summer FY93)
Observation technology experimentation apparatus	In-situ observation of interface and environmental phase during crystal growth (Katsuo Tsukamoto, Faculty of Science, Tohoku Univ; Kazuhiko Kuribayashi (Space Transport Research Group, Institute of Space and Astronautical Science; Tsutomu Sawada, Research Group 13, National Institute for Research in Inorganic Materials)		
Fluid fundamental physical characteristics measuring apparatus	Experiments on generation of Marangoni convection and its control (Hisao Azuma, Space Research Group, National Aerospace Lab (NAL); Akira Hirata, Dept of Science and Engineering, Waseda Univ; Keiichi Kuwabara, Research Lab, Ishikawajima-Harima Heavy Industries, Ltd)		
Microgravity maintaining technology experimentation apparatus	Experiments on generation, growth and movement of bubbles (Nobuyuki Abe, Energy Base Section, Electrotechnical Lab; Masamichi Ishikawa, Advanced Science Research Lab, Mitsubishi General Research Institute; Nobuya Ishii, Takasago Engineering Lab, Mitsubishi Heavy Industries, Ltd)		
General purpose heating equipment	Melting and solidifying experiments of particle-dispersed alloys (Yuji Muramatsu, Research Group No 4, NRIM)	(Not put on board)	Synthesis experiment of ceramic materials (Osamu Odawara, General Science and Engineering Research Lab, Tokyo Institute of Technology)
Temperature gradient type heating apparatus	(not put on board)	Semiconductor growth experiment from molten solution (Sho Nishinaga, Faculty of Engineering, Univ of Tokyo)	Experiment on influence of microgravity on shape of solid liquid interface (Kyoichi Kinoshita, Fundamental Research Lab, NTT)
High temperature heating apparatus	Melting and solidification experiment of oxide superconductors (Kazumasa Togano, Surface and Interface Research Lab, NRIM)	Melting and solidification experiment (Junji Hayakawa, Glass Technology Research Group, Government Industrial Research Institute, Osaka)	(not put on board)

In the following, we will present a summary and results of the "experiment on the melting and solidification of particle-dispersed alloys."

4.2 Summary and Results of "Experiment on the Melting and Solidification of Particle-Dispersed Alloys"

(1) Summary of Experiment

This experiment was carried out with Yuji Muramatsu of the National Research Institute for Metals [NRIM] as the collaborator, aimed at manufacturing high-performance particle-dispersed alloys in which fine ceramic particles are dispersed uniformly through melting and solidification under microgravity.

The manufacturing of a particle-dispersed alloy on the ground is generally done by means of powder metallurgy. Although this method is advantageous for dispersing particles uniformly, the manufacturing process is complicated and the cost of the product is high. It has many problems, such as difficulties with obtaining large products.

The object of this experiment, the significance of which is given below, is to manufacture high performance particle-dispersed alloys by melting and solidification processes under microgravity.

(1) Under microgravity, the separation of a metal and the particles to be dispersed due to differences in specific gravities and the separation due to thermal convection can be suppressed, facilitating uniform dispersion.

(2) Under microgravity, since such effects as surface tension and interface tension become more conspicuous, the elucidation of related phenomena, e.g., wetting and Marangoni convection, can be facilitated.

(3) Since alloys are manufactured exclusively by melting and solidification processes, the problems inherent to conventional powder metallurgy can be eliminated and the manufacture of dispersed alloys can be facilitated. Moreover, the results obtainable by this experiment will be of much utility in the development of other composites and monotectic alloys.

This experiment can be thought of as one in a series of experiments carried out since 1973. This time, in view of the temperature of the furnace to be used during the microgravity period, the experiment will be conducted on the particle-distributed alloys of copper.

The base material is copper (Cu) and the particles to be dispersed are an oxide (Al_2O_3) and a metal (tungsten). The reasons for selecting these two dispersants are that both have high reinforcing properties and hence the product is expected to be promising, that significance (2) above can be demonstrated through the experiment since the wettability with respect to the copper solution differs entirely for each material, etc.

Although the melting point of Cu is 1,083°C, the temperature is raised to a minimum of 1,150°C in order to have melting in a short time, while, in cooling, since solidification takes place by supercooling at temperatures below 1,083°C, it is quickly cooled to the vicinity of 1,000°C.

(2) Results of Experiment

Wettability (conformability) is a very influential factor in the manufacture of particle-dispersed-type alloys and composites. On the ground it is extremely difficult to understand the influence of wettability on the dispersion state since particles and the base material are readily separated due to the differences in density. In order to clarify this

influence, we have carried out the melting and solidification of particle-dispersed alloys under microgravity using a mother phase (copper) and particles with different wettabilities (tungsten particles with good wettability and alumina particles with poor wettability). The internal texture of the samples used in the experiment exhibited conspicuous differences according to the mother phase and wettability of the particle, clarifying the influence of wettability on the dispersed state. From the results, the conclusion was drawn that it is important to improve the particle's wettability to the mother phase in order to achieve uniform dispersion of the particle under microgravity. More specifically, in combination with the poor wettability of alumina/copper, alumina particles were discharged to the surface of the sample. This is because copper and alumina particles repel each other. Furthermore, in a sample in which sufficient time was not available for the alumina particles to be discharged to the surface, an aggregate structure of several to several dozen particles was formed in order for the particles to minimize the contact area with the copper (Figure 4 [not reproduced]). On the other hand, in the tungsten/copper sample, tungsten particles remained inside the copper, forming a structure exhibiting uniform dispersion (Figure 5 [not reproduced]).

5. Materials Experiment on Space Shuttle

5.1 Experiment on Board First International Microgravity Laboratory

(1) Summary

The International Microgravity Laboratory (IML) projects promoted by NASA are aimed at international cooperation in conducting space shuttle/space lab microgravity experiments, with the First International Microgravity Laboratory (IML-1) being the first in a series of IML projects. NASDA has provided two experimental apparatuses for the laboratory and has carried out space experiments. In the IML-1 mission, experiments on 42 topics proposed by 11 countries, including the United States, Canada, European countries and Japan, were carried out over a period of eight days aboard the space shuttle Discovery launched on 22 January 1992 and returned to earth on 31 January.

Japan contributed an organic crystal growth device and a cosmic radiation monitoring device proposed by NASDA.

The experimental topics from Japan are the following two that were proposed by NASDA: (1) "Crystal Growth of Organic Superconductor Under Microgravity," and (2) "Detection and Analysis of High Energy Cosmic Radiation Using Biological Samples."

Here, we will present a summary and the results of experiment (1) only.

(2) Summary and Results of "Crystal Growth of Organic Superconductor Under Microgravity" Experiment

A crystal growth experiment employing the solution diffusion method was carried out utilizing the microgravity environment of the space lab over a period of about one week, aiming at the growth of large high-quality organic superconductors under microgravity and the acquisition of organic crystal growth technology. The experimental apparatus developed for this experiment consists of two sets of three-chamber connection-type crystal growth cells (a vibration controlling member (made of epoxy resin) is provided in one of them), as shown in Figure 6 [not reproduced]. By using microgravity, it was possible to grow an organic crystal of a size comparable to that obtained in ground experiments through a growth experiment of very short duration (approximately 1 week) as compared to approximately 3 weeks on the ground. This was because it was possible to reduce the distance between the chambers for materials, enhance the concentrations of the materials, and markedly reduce the reaction time since, under microgravity, there was no influence of differences in specific gravity or convection.

The space-grown crystals included, in addition to the mutually-welded needle crystals obtained in the ground experiment, excellent crystals with metallic luster and platelike shapes, although they were not large enough (Figure 7 [not reproduced]).

Furthermore, those grown in the cell with a vibration-controlling member generally were slightly larger, confirming the effectiveness of the vibration controller.

Future studies will include structural analysis, measurement of physical properties, etc., by which their quality and properties will be compared with those of the ground-grown crystals to investigate the influence of the lack of gravity on crystal growth.

It should be mentioned that, in connection with this research on organic superconductive crystals, full cooperation was extended to us by Professor H. Anzai, Himeji Institute of Technology, Hyogo Prefecture, I. Kudo, section chief, and chief investigators M. Tokumoto, N. Kinoshita, and K. Murata of the Electrotechnical Laboratory, and K. Honda, Chemical Technology Laboratory.

5.2 EOIM-3

The evaluation of oxygen interaction with materials (EOIM)-3 experiment is a material exposure experiment of which NASA's Johnson Space Center (JSC) is in charge, which is aimed at clarifying the deterioration of the surface material of the space station and low-orbit satellites due to atomic oxygen and measures for preventing it. The EOIM-1 (60 samples by STS-5) and EOIM-2 (300 samples by STS-8) experiments have already been completed.

The EOIM-3 experiment is a large-scale one involving a total of 1,100 samples, of which NASDA is to contribute 46 samples including 26 kinds.

This experiment was carried out using the space shuttle Atlantis, which was launched in July 1992. The specimen was a disk, 1 inch in diameter (2.54 cm), 45 units of which were arranged on a plate approximately 11 cm in width and 33 cm in length. The loading conditions of the specimens on the holder and the payload carrier are shown in Figure 8 [not reproduced]. In addition, the names of the 26 kinds and 46 units ultimately selected are given in Table 2, with their configuration given in Figure 9 [not reproduced]. These specimens were exposed to space for approximately 40 hours under the conditions of an orbital altitude of about 222 km and orbital inclination of 28.5°. The irradiation amount of atomic oxygen has been estimated to be approximately 2×10^{20} atoms/cm^2.

Table 2. Names of Test Pieces Put On Board

Use	Item Name	Manufacturer/Type Name	Quantity Put On Board	Tray Address
Heat Control Material	Aluminum/polyester	(Scherdahl)/G405310	2	12, 35
Same	Aluminum/polyester	Kanegafuchi Chemical Co/KF-25S	2	01, 24
Same	Aluminum/polyimide	(Scherdahl)/G405110	2	28, 39
Same	Aluminum/polyimide	Ube Industries Ltd/ Upilex-25R Al- deposited	2	06, 29
Same	Polyimide	Nitto Denko/(Nitmid) U-film N-type	1	40
Same	Polyimide	Ube Industries/Upilex 25S	1	16
Same	ITO/polyimide/Al	Ube Industries/ITO/ Upilex 25R/Al	2	09, 20
Same	White paint	(Yttry)/S13G/LO	1	17
Same	White paint	Whittaker/APA2474	1	38
Same	Black paint	Lord/Chemiglaze 306	2	02, 13
Same	OSR (optical solar reflector)	(Pilkinton)/PS219	3	44,33,10
Exposed Structural Material	CFRP	Toray/Mitsubishi Electric Co/T800/FWR-1	3	04,15,26
Same	CFRP	Toray/Mitsubishi Electric Co/M40/FWR-1	3	14,25,37
Same	Matrix	Mitsubishi Electric Co/ FWR-1	2	03, 36
Insulating Material	PFA	Japan Vulcar/(Vulfreon)	2	43, 32
Same	ETFE	Japan Vulcar/(Vulfreon)	2	08, 19
Same	PTFE	Japan Vulcar/(Vulfreon)	1	18
Same	PVdF	Japan Vulcar/(Vulfreon)	2	42, 31
Adhesive	Silicone resin	GE/RTV-142	2	07, 30
Same	Silicone resin	GE/RTV-566	1	41
Same	Conductive epoxy resin	Grace/ECCOBOND 56C	2	05, 27
Optical Material	ZnS coating	Matsushita Engineering Research Lab/MRIT-K-007	2	23, 46
Same	SiO coating	Hitachi Optical Co/MR-AS-400	2	11, 34
Same	MgF_2 coating	Fuji Photographic Industries Co/FS	1	22
Same	Cover glass	Asahi Glass Works, Ltd/AS-150	1	21
Same	Cover glass	(Pilkinton)/CMX	1	45

Following the return of the space shuttle, the recovered specimens' surface properties will be measured, sections will be observed, etc., within Japan and will be reported at a NASA meeting next year, which will be followed by a comparison with NASA's report.

5.3 First Material Processing Test Project (First Materials Experiment)

(1) Summary

The project was carried out using the space shuttle Endeavor and the space lab launched on 12 September 1992 from Kennedy Space Center. After the space shuttle began orbiting the earth, a total of 34 topics, consisting of 22 materials experiments and 12 life science experiments which are difficult to perform on the ground, were carried out by Mamoru Mori, payload scientist (PS), using numerous apparatuses. The entire mission, including seven American experimental topics, two U.S.-Japan joint experimental topics, etc., was called Space Lab J (SL-J). The 22 materials experiment topics are shown in Table 3. The results of these experiments will be analyzed and summarized by the respective proposers of the topics.

Table 3. Summary of 22 Material Test Topics for First Material Processing Test Project

Topic	Scientist in Charge	Purpose
(M-1) Growth of Narrow-Band-Gap Lead, Tin and Tellurium Ternary Mixed Crystal Semiconductor Single Crystal Under Microgravity	Tomoaki Yamada (Fundamental Research Laboratory, NTT)	To manufacture a homogeneous composition and defect-free single crystal of narrow band gap lead, tin and tellurium ($Pb_{1-x}Sn_xTe$) ternary mixed crystal semiconductor which is expected to be applied as a far infrared laser element by the Bridgman method under microgravity. A high-quality single crystal is difficult to obtain on the ground because of the inhomogeneous composition resulting from thermal convection, etc.
(M-2) Experimental Manufacturing of Large PbSnTe Single Crystal by Zone Melt Method Under Microgravity	Shohachi Iwai (The Institute of Physical and Chemical Research	To grow a large single crystal of lead, tin and tellurium (PbSnTe) of uniform structure, which shows promise as a material for infrared emission and photodetector elements and which is difficult to manufacture on the ground due to problems with component separation.
(M-3) Manufacture of Compound Semiconductor Crystal by Floating Zone Melt Method	Isao Nakaya (National Research Institute for Metals (NRIM), STA)	To demonstrate the possibility of growing large high-quality single crystals of indium-antimony (InSb) under microgravity, the manufacturing of which on the ground by the floating zone melt method is extremely difficult due to the high density and low surface tension.
(M-4) Fused Manufacture of New Superconductive Alloy	Kazumasa Togano (Tsukuba Station, NRIM, STA)	To manufacture under microgravity an ingot of an aluminum-lead-bismuth alloy (Al-Pb-Bi).which has excellent flexibility and shows promise as a fiber-dispersed-type superconductive wire in which the lead-bismuth alloy is dispersed uniformly in the mother phase of aluminum.
(M-5) Formation Mechanism of Deoxidation Products in Compositely- Deoxidized Steel Ingot	Akira Fukuzawa (NRIM, STA)	To deoxidize an iron and iron-10% nickel alloy (Fe-10%Ni) ingot by deoxidizing agents of single systems of aluminum (Al), silicon (Si) and manganese (Mn) and their composite systems to investigate the components and distribution of deoxidation products which are not known on the ground due to thermal convection and buoyancy, and to confirm the formation mechanism.
(M-6) Manufacture of Particle-Dispersed-Type Alloy	Yuji Muramatsu (NRIM, STA)	To manufacture a high-strength, heat-resistant alloy with uniform particle dispersion and no voids by melting, pressurizing and cooling the uniformly-mixed powder of nickel (Ni) alloy particles, that become the mother phase, and ceramic particles such as alumina (Al_2O_3) and titanium carbide (TiC) under microgravity where no thermal convection or buoyancy exist.
(M-7) Mutual Diffusion of Two Kinds of Melted Metals, and Texture and Structure of Alloys and Compounds Formed by Solidification	Takehiro Dan (NRIM, STA)	To obtain knowledge of mutual diffusion, nucleus formation, and crystal growth by melting a sample by joining metallic bars of gold and silver under microgravity where disturbances due to thermal convection are absent.
(M-8) High-Temperature Behavior of Glass	Naohiro Soga (Faculty of Engineering, Kyoto University)	The main object is to obtain accurate data on density and volume changes of glass in a high temperature state by optically measuring the diameter of a glass ball based on the fact that the shape is retained due to surface tension even when a spherical sample of oxide glass is softened and melted under microgravity.
(M-9) Growth of Spherical Silicon Crystal and Its Surface Oxidation	Sho Nishinaga (Faculty of Engineering, Tokyo University)	To manufacture an ideal silicon single crystal by growing it spherically under microgravity without subjecting it to directivity to clarify its growth mechanism. In addition, by oxidizing the surface of the sphere on the ground, the properties of the substrate and the oxide layer can be investigated.
(M-10) Research on Solidification and Growth of Unmixable Alloy Systems	Akihiko Kamio (Faculty of Engineering, Tokyo Institute of Technology)	Monotectic unmixable alloys, such as aluminum-indium (Al-In), aluminum-lead-bismuth (Al-Pb-Bi), and copper-lead (Cu-Pb), are melted and mixed under microgravity to obtain a monotectic alloy with homogeneous orientation which cannot be obtained on the ground.
(M-11) Research on Manufacturing High Rigidity and Ultra-Low Density Carbon Fiber/Aluminum Alloy Composite	Tomoo Suzuki (Faculty of Engineering, Tokyo Institute of Technology)	To manufacture a composite with low density and high rigidity by melting in zero gravity only the clad layer of an aggregate of short carbon fibers coated with aluminum. This material is useful in space as a structural material.
(M-12) Research on Liquid Phase Sintering Mechanism	Tsuguro Ohara (Faculty of Fundamental Engineering, Science University of Tokyo)	To confirm theoretically the liquid phase sintering mechanism by subjecting a mixed powder of spherical particles of tungsten (W) and nickel (Ni) under microgravity, and by growing grains in the state in which solid particles of tungsten are dispersed uniformly in the liquid phase of nickel.

Table 3. Summary of 22 Material Test Topics for First Material Processing Test Project (Continued)

Topic	Scientist in Charge	Purpose
(M-13) Structure of Si-As-Te Amorphous Semiconductor Under Microgravity	Yoshihiro Hamakawa (Faculty of Science, Osaka University)	To manufacture a highly homogeneous and high quality sample of a silicon-arsenic-tellurium (Si-As-Te) amorphous semiconductor with a wide range of applications as a new optoelectronic element.
(M-14) Research on Vapor Phase Metallic Coagulation Mechanism Under Microgravity	Nobuhiko Wada (Faculty of Science, Nagoya University)	To form fine particles by evaporating, diffusing and coagulating silver (Ag) in a rare gas sealed in an experimental sphere, under microgravity with no convection, and to record the process and confirm the formation mechanism.
(M-15) Behavior of Liquid Drop in Acoustic Floating Device and Research on Acoustic Wave Interference History	Hisao Azuma (National Aerospace Laboratory (NAL), STA)	To measure the natural properties and acoustic wave interference of a liquid drop by letting a liquid drop float in microgravity in space. Moreover, will observe the deformation and splitting mechanism by putting the floating liquid drop into rotation or motion to study the noncontact manipulation technology of the liquid drop.
(M-16) Clarification of Behavior of Bubble in Field with Temperature Gradient and Ultrasonic Standing Wave	Hisao Azuma (NAL, STA)	The behavior of a bubble under microgravity is thought to be quite different from that on the ground, and the clarification of such a phenomenon is important in creating materials, etc., in space. This experiment will observe such things as the behavior of air bubbles and liquid bubbles in a field with a temperature gradient, and of an air bubble in an ultrasonic wave.
(M-17) Research on Optical Materials for Invisible Region	Junji Hayakawa (Government Industrial Research Institute, Osaka, AIST, MITI)	To obtain a glass lump having the high purity and high transmissivity necessary for an optical material for the invisible region (infrared region) by melting the raw material of glass without contacting a container, thereby preventing crystallization and contamination.
(M-18) Research on Marangoni Convection in Material Manufacturing Process Under Microgravity	Shintaro Shioji (Technical Research Laboratory, Ishikawajima Harima Heavy Industries, Ltd.)	To observe the flow situation of aluminum powder added to an eicosane sample in order to investigate the influence of the Marangoni convection, which is thought to have an important influence on the growth process of crystals and structures, during the coagulation of melted materials.
(M-19) Research on Coagulation of Eutectic Alloys Under Microgravity	Atsumi Ono (Chiba Institute of Technology)	To confirm the formation mechanism of free crystals by melting and coagulating eutectic alloys under microgravity where convection does not exist.
(M-20) Synthesis of Samarskite Under Microgravity	Shunji Takegawa (Research Institute for Inorganic Materials, STA)	To obtain single crystal sample by growing a crystal using the floating zone melt method in a microgravity environment, which lacks thermal convection and gravity segregation, using the raw materials for samarskite, which is a multicomponent compound believed to have existed on earth, but which is difficult to reproduce on the ground.
(M-21) Growth of Organometallic Crystals Under Microgravity	Hiroyuki Anzai (Electrotechnical Laboratory, AIST)	To grow a large high-quality single crystal, under microgravity, with properties not found in conventional metals, utilizing diffusion which is not hampered by precipitation or convection.
(M-22) Manufacturing Compound Semiconductor Under Microgravity (Research on InGaAs)	Masayoshi Tatsumi (Fundamental Research Lab, Sumitomo Electric Industries, Ltd.)	To manufacture, under microgravity, a uniform- composition single crystal of indium-gallium-arsenic (InGaAs) by unidirectional solidification, which is difficult to manufacture on the ground due to thermal convection but which is expected to be useful as an optoelectronic material.

The experience gained in the project is expected to serve as a valuable resource in promoting development related to space experiment technology and manned space technology directed toward future space station projects.

5.4 Experiments To Be Conducted On Board the Second International Microgravity Laboratory (IML-2)

The goals of IML-2 are to participate in the IML series through international cooperation, as proposed by NASA, based on the results of the space experiments conducted by IML-1 and this project, and to accumulate technology and experience for the development of common technology and apparatus for space experiments through the provision of the apparatus to be used in the space experiments.

The plan is for the IML-2 space experiments to be carried out aboard the space shuttle Columbia scheduled to be launched in July 1994, in which NASA, Japan, the European Space Agency (ESA), Germany, Canada and France are expected to participate. In 1989, NASA selected the experimental apparatus to be placed on IML-2, with Japan assigned to propose topics using six kinds of apparatus. In response to this, NASDA solicited experimental topics that would use these apparatuses. A total of 75 topics were submitted from industry, academia and government, of which 12 were selected. Two materials experiments topics have been selected, which are summarized in Table 4.

Table 4. Summary of IML-2 Materials Test Topics

Topic	Scientist in Charge	Object	Experimental Apparatus
Composition Control of TiAl-Based Intermetallic Compound	Masao Takeyama (NRIM, STA)	To manufacture uniform composite of titanium-aluminum alloy, which is a lightweight and high-strength metal, and titanium and boron fine particles, ultimately creating high-strength reinforced materials.	High-temperature pressurization-type electric furnace
Uniform Dispersion and Mixing of Compound Semiconductor Fused Solutions	Akira Hirata (Waseda University)	To aim at materials manufacturing technology by positive use of Marangoni convection, which becomes conspicuous under microgravity, realizing ternary semiconductor materials with different densities as the object.	High-temperature pressurization-type electric furnace

It should be mentioned that, on 19 October 1992, Chiaki Mukai of NASDA was officially selected as the payload scientist (PS) for this experiment.

6. International Space Station Project

The space station project is a multipurpose manned facility to be constructed in an earth orbit mainly using the space shuttle. This project, for which design development has been in progress since 1988 following the completion of preliminary designs in 1985, is to be carried out through international cooperation among the United States, ESA, Canada and Japan, and is scheduled to be completed by the end of this century, as was mentioned earlier.

The space station project consists of a station main body, which will orbit the earth at an altitude of approximately 400 km and an inclination angle of approximately 28.5 degrees, a supporting manned free flyer to be provided by ESA, and polar orbit platforms that will enter polar orbits of altitudes of approximately 700 km and which are to be supplied by NASA and ESA, as shown in Figure 10 [not reproduced]. The station main body will be constructed as a permanent manned space facility to be operated for about 30 years, and will consist of components that will be provided by the international partners. The overall view of the station main body is shown in Figure 11 [not reproduced].

The United States will participate in the project by providing the infrastructure of the space station main body, a polar orbit platform, and related ground facilities, including a space station control center, payload operation general center, etc. Japan will participate by providing an experimental module (Japanese Experimental Module (JEM)) to be attached to the station main body for carrying out materials experiments, life science experiments, celestial and earth observation, scientific and engineering experiments, and communications experiments. ESA will be in charge of providing an experimental module (attached pressurized module (APM)), a polar orbit platform, a manned support-type free flyer (MTFF) with a pressurized structure which will normally be unmanned, but which can accomodate astronauts when needed, and the related ground facilities (ESA summarizes these as the "Columbia Project"). Canada will participate by providing a mobile service facility (manipulator for space station), reflecting the development record of the manipulator for the space shuttle.

7. Experimental Module "JEM"

7.1 Summary of JEM

The full-scale development of JEM was begun in January 1990. The development and operational schedule of JEM is shown in Figure 12 [not reproduced]. As shown in Figure 13 [not reproduced], JEM consists of a pressurized module (PM), an exposed facility (EF), an experiment logistics module-pressurized section (ELM-PS), a remote manipulator system (RMS), and an experiment logistics module-exposed section (ELM-ES). These are to be assembled in orbit through the concerted efforts of the space station manipulator (SS RMS) and JEM RMS, with the pressurized module coupled on the side of the station main body, of which NASA is in charge. Accordingly, the crew working inside JEM can commute between the JEM PM and ELM-PS without wearing space suits, the same as in the space station main body. In addition, a manipulator for supporting experiments in the EF and an air lock for transferring samples for experiments, etc., in the EF are attached to the PM. The principal dimensions are shown in Table 5.

Table 5. Principle Dimensions of JEM

Dimensions	Pressurized Module	Experiment Logistics Module		Exposed Facility
		Pressurized Section	Exposed Section	
Shape	Cylindrical	Cylindrical	Frame type	Box type
External form	approx. 4.2 m φ	approx. 4.2 m φ	4.5 m (W) x 3.5 m (H)	5.0 m (W) x 3.7 m (H)
Total length	approx. 9.9 m	approx. 4.1 m	approx. 1.8 m	approx. 5.3 m
Weight	approx. 14.7 t	approx. 2.4 t	approx. 0.7 t	approx. 2.9 t
Mission payload number	10 payload racks	8 racks for pressurized module	3 payload racks	10 payload racks
Power (maximum mean)	Maximum 25 kW dc 120 V			
Data transmission	10 Mbps (payload network); 100 Mbps (high speed data)			

The interior sub-system equipment in the pressurized module has been configured for controlling the air constitution, temperature and air circulation, and for managing and controlling the heat adjustment, power supply, communications, etc., for the entire JEM in order to enable manned experimental activities to be conducted in a pressurized environment. On either wall surface are 10 experimental racks for housing experimental equipment, a work station for the crew to centrally control JEM, and a work bench for supporting maintenance and experiments. In addition, a manipulator console and a direct-view window are provided in the rear end of the side on which the EF is attached. A protective board for protecting the PM from fine meteorites is attached to the periphery of the PM drum.

The exposed facility is where experiments are carried out in an exposed environment and where up to 10 payload items for experiments can be attached to the basic body of a box-type structure by means of an equipment exchange structure. Apparatuses for the power supply, communications control and heat radiation are installed inside the basic body. Moreover, a configuration that takes the operation of the manipulator into account is provided for the layout and equipment interface since the principal moving of equipment over the EF is done by the manipulator.

The experiment logistics module carries supplies for the JEM and goes back and forth between the space station and the ground. The pressurized section mainly transports experimental equipment, samples for experiments, system supplies, etc., and is also used for storage in orbit. The exposed section is used for transporting experimental equipment in the EF, and is generally attached, in orbit, to the rear end of the EF.

The remote manipulator system consists of a host arm, with a slave arm attached to its tip. The host arm has a total length of approximately 10 meters, while its tip has a tip pinching part common to the RMS for the space station, and is normally used for attaching and exchanging payloads for the EF. The slave arm is used for small operations or for jobs requiring dexterity, such as exchanging experimental samples, supporting structure assembly testing, maintaining and exchanging EF subsystems, etc.

7.2 Utilization and Operation of JEM

As for the space station, which is aimed at operating in orbit, investigations of the work in fields related to the (1) launch site and launching, (2) assembly in orbit, (3) steady operation and (4) supplies, etc., are in progress by the various countries, centered around NASA. NASA is in charge of assembling the entire space station and the related training, data transmission via TDRS (NASA data relay satellite), supply and recovery (at 90-day intervals) by the shuttle, etc., and each country is responsible for the verification, training, maintenance and security of the elements it has developed.

The overall operation of the entire space station is being taken care of by NASA JSC's space station control center, while the overall operation of the experimental apparatus will be handled by the Marshall Space Flight Center (MSFC). As for Japan, an operation center is to be established at Tsukuba Space Center to independently monitor and control JEM to the maximum extent possible and to control experiments and carry out data processing.

The concept of the JEM operation system is shown in Figure 14 [not reproduced].

The mode of operation will be such that, although during the initial period each user will mainly carry out his own experiments using the common experimental equipment, with the accumulation of experience in space experiments it is anticipated that the development and use of individual experimental equipment will take place, and it is expected further that this will develop into commercial applications and industrialization. Moreover, a pre-announcement of opportunity (Pre-A.O.) for JEM utilization took place in mid-1990 to prepare for utilization, with the first topic solicitation (A.O.) for JEM utilization publicized on 1 October 1992. Although the first announcement was limited to experiments within the PM, experiments in the EF will be an additional goal of the second A.O. scheduled for October 1993.

7.3 Crew for JEM

The space station operation will initially be undertaken by a crew of four. After the power has been increased to 75 kW as a result of the subsequent stepwise development, and with the addition of NASA's living quarters, an increase in the emergency return ship capacity, etc., the number of crew members is planned to be increased to eight. The crew will consist of a station commander (SC), station operator (SO), station scientist (SS) and payload scientist (PS). The crew will stay in the space station for 3 to 6 months, with half of them replaced every 3 months. The ratio of Japanese crew members will be approximately one-eighth, based on the agreement document, etc.

The criteria for the JEM crew selection includes, in addition to the general aptitude for official, basic quality requirements, such as the course of study, experience, proficiency in English, etc., and psychological aptitude, the NASA Class 2 Medical Selection Criterion, etc. Regarding the selection of a JEM astronaut, the first to third selection rounds took place from September 1991 to March 1992 in order to judge the adaptability of the candidates. On 1 June 1992, Koichi Wakata was selected as a candidate for a JEM crew member. He is currently receiving training at Johnson Space Center.

8. Conclusion

The no-gravity environment of space is expected to open great possibilities for new materials development, which is difficult to realize on the ground where gravity prevails. Japan's materials experimentation under a space environment, which started with one on a small rocket, has advanced to the materials experiments conducted by NASDA PS Mamoru Mori on board the American space shuttle Endeavor. These technical results are expected to be taken over and expanded by materials experiments aboard the space station.

Although the full-scale utilization of the space environment represents a new frontier which has just begun, numerous needs exist and, hence, interest not only in materials experiments, but also in other fields is expected to be raised.

Design of Heat-Resistant Alloys

936C1023D Tajimi CHO KO ON ZAIRYO SYMPOSIUM '92 in Japanese 3 Dec 92 pp 41-49

[Article by Masahiko Morinaga, Toyohashi University of Technology; English abstract provided by source]

[Text]

[Abstract]

Recently, a new alloy design method has been developed based on molecular orbital calculations. With this method, two alloying parameters are calculated and used to understand alloy properties. One is the bond order and the other is the d-orbital energy level. The phase stability of austenitic alloys is quantitatively predictable with these alloying parameters. Also, a target region for alloy design can be specified concretely in the coordinates of these parameters. This method has been applied successfully to the design and development of single crystal Ni-based superalloys. In addition, the structural stabilities of refractory bcc metals, including Nb and Mo, have been found to be correlated with the bond order. The mechanical properties of intermetallic compounds are also discussed in terms of the nature of the electronic bond between atoms.

1. Introduction

In order to enhance the thrust and efficiency of jet engines, it is necessary to raise the temperature of the gas at the turbine inlet. For this reason, ultra-high-heat-resistant alloys that excel in high-temperature strength and corrosion resistance have been developed successively.[1] Of these ultra-high-heat-resistant alloys that can roughly be divided into Fe-based, Co-based and Ni-based alloys, the Ni-based alloys, which have excellent toughness and high-temperature strength, are mainly used for rotor and stator blades of turbines, which are exposed to the most severe conditions.

In the past, the development of Ni-based ultra-high-heat-resistant alloys has been done by relying on a considerable amount of trial-and-error experience over long periods of time. Because of this, enormous sums of funds and expenses were required for alloy development. "Alloy design" was first proposed for this type of alloy as an effective alternative. Namely, approximately 30 years ago, a prediction method (PHACOMP) was proposed for the formation of harmful brittle phases (σ or μ phase) which appear during the use of Ni-based heat-resistant alloys.[2],[3] Actually, it is a historical fact that the term "alloy design" was first used following the development of this method.

Moreover, recent thought has been that the development of such alloys as Nb- based or Mo-based ones based on the so-called refractory bcc metals is indispensable for the development of next-generation nuclear reactors (e.g., the portable fast breeder reactor).

In this article, we will present the "d-electron alloy design method"[4]-[6] proposed by the author for the design of heat- resistant alloys, as well as ideas concerning the future design of heat- resistant alloys.

2. d-Electron Alloy Design Method

The physical and chemical properties of metals and alloys are closely related to the behavior of the electrons contained in them. Accordingly, it is necessary to understand a material from the microscopic standpoint on the electronic level. In other words, a theoretical material design based on calculations of the electronic structure is strongly desired. The author and his colleagues have derived the alloy parameters to be used to estimate the properties of alloys from molecular orbital calculations.[4]-[6] Although it may be contrary to one's expectations, such parameters reflecting the alloying effect have so far hardly been recognized, in spite of the long history of the study of metals.

2.1 Molecular Orbital Calculation

Although there are various types of molecular orbital calculations, a method closest to the first principle is desirable. The author's group has simulated the local electronic state around the alloying element by means of the DV-Xα cluster method.[7] Here, the term "cluster" refers to an imaginary molecule in a crystal. For example, Figure 1 [not reproduced] is a cluster model used for calculating metals with a face-centered cubic lattice, such as nickel. By varying the alloying amount M at the center, the chemical bond between M and the mother metal X is investigated. In this way, the alloying parameter that represents the personality (i.e., the alloying effect) exhibited by M in the mother metal is determined.

2.2 Alloying Parameters

The kind of parameter that should be employed depends, of course, on the way the alloy is used. However, if it is restricted to structural materials, then the following two parameters will be useful.[8],[9]

One of them is the bond order (Bo). As shown in Figure 2 [not reproduced], this is a parameter which shows the degree of overlap of the mother metal element X and the alloying element M. The bonding between the atoms of M and X is stronger for a larger bond order. The other is the d orbital energy level (Md) of the alloying element M. Since, in the case of a transition metal, the behavior of the d electron is important, such a parameter is used. As shown in Figure 2(b) [not reproduced], Md has to do with the electron negativity and atomic radius of an atom. In fact, it is known that the energy level determined by the Xα method is none other than the electron negativity.[5]

As an example of the calculated results, the Md and Bo values of various elements determined for Ni alloys are shown in Table 1.[10] These values have also been obtained for other alloys. We would like to especially emphasize here that these values have been derived as parameters representing, for the first time, alloying characteristics by molecular orbital calculation.

Table 1. List of Bo and Md Values for Ni Alloys

	Element	Md (eV)	Bo
	Ti	2.271	1.098
	V	1.543	1.141
	Cr	1.142	1.278
	Mn	0.957	1.001
3d	Fe	0.858	0.857
	Co	0.777	0.697
	Ni	0.717	0.514
	Cu	0.515	0.272
	Zr	2.944	1.479
4d	Nb	2.117	1.594
	Mo	1.550	1.611
	Hf	3.020	1.518
5d	Ta	2.224	1.670
	W	1.655	1.730
	Re	1.267	1.692
	Al	1.900	0.533
	Si	1.900	0.589

In general multicomponent alloys, the average over the composition is taken as a first approximation to define the means Bo and Md, i.e., Bo (mean) = ΣXi x (Bo)i, and Md (mean) = ΣXi x (Md)i, where Xi is the atomic fraction of the alloying element i, while (Bo)i and (Md)i are its Bo and Md values, respectively. For nickel alloys, the values in Table 1 must be used.

Since the era of Pauling, the chemical bond between atoms has been represented in terms of such parameters as the size of the atom and the chemical negativity. In metallic materials, as well, these parameters have been used to understand such basic problems as the solid solution limit and the crystal structure of alloys. In comparison to these classical parameters, Bo and Md are parameters that are determined directly from cluster calculations of alloys, and are related to various properties of alloys.

3. Evaluation of Alloy Characteristics by Alloy Parameters

In the following, the utility of these parameters in understanding metallic materials will be demonstrated using several examples.

3.1 New PHACOMP

If brittle phases such as the σ phase and the μ phase appear in a heat- resistant alloy for high temperatures, its mechanical properties deteriorate markedly. As a method for estimating the generation of these embrittlement phases, PHACOMP (phase computation) has been invented.[2],[3] This is a method which is still being used worldwide as the manufacturing specifications for nickel-based ultra-high-heat-resistant alloys or as a measure for alloy development. With this method, use is made of the number of electron vacancies (Nv) as the parameter. As shown in Figure 2(c) [not reproduced], Nv is the number of electron vacancies found in levels above the Fermi level in the d-band. In alloys, Nv's compositional mean is taken. If Nv (mean) exceeds a certain critical value, it is predicted that an embrittlement phase will precipitate.

However, there are various discrepancies in this empirical Nv- PHACOMP.[4],[5] For example, (1) some alloy systems exist which do not permit the generation of the principal embrittlement phase, i.e., the σ-phase, of Ni-based alloys to be estimated, (2) it is not possible to estimate the generation of embrittlement phases other than the σ-phase (μ-phase, Laves phase, etc.), and (3) it is difficult to apply it to heat-resistant alloys other than Ni-based ones, such as Co- and Fe-based alloys, etc. Although various improved methods[11] have been proposed, since many of the discrepancies originate from the Nv parameter itself, they have not led to any essential solutions. The author and his colleagues noticed that the parameter Md is correlated to such parameters as the electron negativity and the atomic radius that have been used in explaining the phase stability of alloys. Using Md, they found that the phase boundary of the mother phase, i.e., the γ (fcc) phase, and the second phase (e.g., σ, μ, γ'(Ni_3Al), β(NiAl) phase, etc.) of austenitic alloys can be represented nicely.[12] An example of the results is shown in Figure 3 [not reproduced]; Figures 3(a) and 3(b) are isothermal phase diagrams for Ni-Co-Cr and Ni-Cr-Mo systems, respectively, at 1477 K. The σ phase appears in both of these phase diagrams. The boundary between the γ phase and the (γ + σ) phase can be represented by a line Md = 0.925 (eV—the unit eV will be omitted hereafter). On the other hand, the line corresponding to Nv (mean) = 2.49 that has been used conventionally is fairly far removed from the phase boundary in both Figures 3(a) and 3(b). In the figure, R (mean) is the compositional mean value of the atomic radius. The line for R (mean) = 1.264 (10^{-10} m) runs along the phase boundary in Figure 3(a), but does not in Figure 3(b). As in the above, in contrast to the conventional PHACOMP, which uses (e/a) and assumes a rigid band model, the parameters determined by molecular orbital calculations can explain some of the actual phase diagrams fairly well.

The results of estimating embrittlement phase generation are summarized in Figures 4(a) and 4(b) [not reproduced] for Ni-based practical alloys and Figures 4(c) and 4(d) [not reproduced] for Co-based practical alloys.[12] For Ni-based alloys, according to estimates by Nv (mean) in Figure 4(b), the boundary for σ-phase precipitation has a width that extends over the range of from 2.15 to 2.30. Barrows and Newkirk tried to remove this defect of the Nv (mean) method under various assumptions, but the problem still remained in IN713C and IN713LC. On the other hand, according to the method using Md (mean) shown in Figure 4(a), the precipitation boundary is at 0.915, and the σ phase is precipitated in alloys with an Md (mean) exceeding this value.

Figures 4(c) and 4(d) [not reproduced] show the estimated results for the embrittlement phase as analyzed by Sim's method.[13] The Nv (mean) value that shows the embrittlement phase-generating boundary given for Co-based alloys is approximately 2.70. However, as shown in Figure 4(c), the phase appears at a considerably lower value than this, for example, in L-605. On the other hand, in Figure 4(d), the boundary is in the vicinity of Md (mean) = 0.90, and the presence or absence of the embrittlement phase is clearly classified in this figure.

As in the above, the conventional method of estimating the embrittlement phase by Nv (mean), i.e., Nv-PHACOMP, is not effective enough. The Md- PHACOMP can also be applied to Co-based alloys. Accordingly, a unified evaluation of the phase stability of austenitic heat-resistant alloys becomes possible with the present method.

3.2 Target Region of Nickel-Based Alloys and Solvus Temperature of γ' Phase

In the past, various kinds of Ni-based ultra-high-temperature-resistant alloys have been manufactured. Figure 5 [not reproduced] plots the 0.2 percent yield stress of the conventionally-cast nickel alloys ((1)-(19)) on the Bo-Md diagram.[14] In the figure, the contour line for the 0.2 percent yield stress is shown as a broken line. Empirically-manufactured alloys have been gradually improved. Interestingly enough, these alloys congregate in the vicinity of Md (mean) = 0.98 and Bo (mean) = 0.67. The single crystal alloys which have become the focus of attention lately exist in this region, as shown in the figure. In this way, the target regions of alloy design exist in a certain limited region of the Md (mean)-Bo (mean) diagram.

In the same figure [not reproduced], the locations of Ni-10 mol percent M binary alloys are indicated by vectors. The origin of the vectors is the location of pure nickel. For metals whose positions in the periodic table are close to that of Ni, such as Co, the magnitude of the vector is small since there is not much difference between its Bo and Md values. On the other hand, since metals such as Hf and Zr have Bo and Md values that differ significantly from those of Ni, the magnitude of their vectors is very large. Interestingly enough, vectors for metals in the same group of the periodic table, e.g., Ti, Zr, Hf (group 4A), V, Nb, Ta (group 5A) and Co, Mo, W (group 6A), point in nearly the same direction. In alloy design, alloy compositions are calculated for combinations of the alloying vectors whose resultant vectors fall in the target region of the Bo (mean)-Md (mean) diagram.

Figure 6 [not reproduced] shows a result of the configuration of the γ'- phase solvus temperature on the Bo (mean)-Md (mean) diagram.[14] The γ'-phase is an intermetallic compound of the Ni_3Al type, and it reinforces the alloy by being precipitated in the γ-phase. In alloys manufactured recently, the volume fraction exceeds 60 percent. Therefore, the stability of the γ'-phase is indispensable for Ni-based alloys as high temperature materials. At temperatures above the solvus temperature, the γ'-phase becomes unstable and dissolves in the mother phase. Therefore, this temperature is of significance to the Ni-based alloys. As shown in Figure 6 [not reproduced], the line for the equisolvus temperature moves toward the high Md (mean) and low Bo (mean) sides as the temperature rises. The slope of the equisolvus temperature line lies between the slopes of the Ni-W and Ni-Ta alloy vectors. Therefore, it can be seen that the addition of V, Nb, Ta, Ti, Zr, Hf and Al raises the γ' solvus temperature of the alloys. On the other hand, the addition of Co, Re, Cr, Mo and W lowers the γ' solvus temperature. This has been confirmed by experiments. For example, it can be seen from Figure 7 [not reproduced] that the γ' solvus temperature rises with an increase in the component ratio Ta/W.[14] The fact that the change of the γ' solvus temperature decreases for a component ratio greater than 1.1 is due to the alloy being in the γ + γ' eutectic region. From this figure, it is also clear that the precipitated amount of the γ' phase increases monotonically with the Ta/W component ratio.

As mentioned earlier, the target region of alloy design is limited to a quite narrow region. Such a region can be understood as that most favorable for raising the γ' solvus temperature as much as possible and increasing the precipitation amount of the γ'-phase, while keeping the phase stability at a desirable level.

3.3 Phase Stability Index Diagram for Austenitic Steels

When an iron-based austenitic steel is annealed from a high temperature, various metallic structures appear depending on the composition.[15] Figure 8 [not reproduced] diagrams an index for estimating the annealed structural conditions. This diagram can also be used for estimating high manganese steels which are difficult to predict by means of the Scheffler diagram, which has conventionally been in widespread use. The region of the appearance of the undesirable σ-phase, when aged at 1073K after annealing, is also specified. For reference, the target region of an Fe-Mn alloy for the wall of a low-radiation nuclear fusion reactor is indicated in the figure.

4. Theoretical Design of Nickel-Based Single Crystal Heat-Resistant Alloys

Alloy design was carried out by taking into consideration the manufacturing conditions for single crystals and using a new PHACOMP for the region shown in Figure 5 [not reproduced] under conditions in which no brittle compounds appear. As shown in Figure 9 [not reproduced], the five basic properties of creep fracture life, fracture elongation, corrosion resistance, density and material cost are better balanced in the designed alloys (TUT92 and TUT 95) than in other single crystal alloys.

Figure 10 [not reproduced] shows the locations on the Bo (mean)-Md (mean) diagram of the single crystal alloys manufactured so far.[14] This figure, which shows enlarged diagrams of the single crystal parts of Figure 5 [not reproduced], indicates that all of the promising alloys manufactured to date are aggregated in the vicinity of Bo (mean) = 0.665 and Md (mean) = 0.985. For example, in PWA alloys, the PWA1484 alloys of (h) in this region were developed by improving PWA1480 at (u), which is located far from this region. In addition, in the CMSX alloy, the improvement of (g) → (m) and (n) was carried out so as to bring (g) closer to the region. The TUT92 alloy at (k) developed by the author's group also lies in this region. However, the TUT95 alloy at (r) lies at a location which is somewhat removed. As in this case, the current situation is that the target region for the single crystal alloys has not yet been pinpointed. However, there is no doubt that the Bo (mean)-Md (mean) diagram is an important index for the development and improvement of alloys.

5. bcc Fire-Resistant Metals and Their Alloys

The bcc fire-resistant metals show promise as the future structural materials for nuclear reactors. For example, Nb- and Mo-based alloys are candidate materials for the portable fast breeder reactor.

The results of the bond orders calculated for various bcc metals are shown in Figure 11 [not reproduced].[17] All

curves demonstrate similar changes for the alloying metal M. In this case, when the mother metals are Nb, Mo, V, Zr, Ti and Fe, the addition of the alloying element M brings about similar effects. Moreover, the value of the bond order is greater for mother metals Nb, Mo and V than for Zr, Ti and Fe. Although the latter metals are those which undergo allotropic transformation of bcc → fcc → bcc, or hcp, the former metals are stable bcc metals at all times and do not undergo allotropic transformation. In other words, it can be seen that the crystal structure of metals demonstrating strong bonding in the bcc state does not change, while the crystal structure of metals exhibiting weak bonding tends to change at a certain temperature. As shown in Figure 12 [not reproduced], the bond order is related to the activation energy (Q) for diffusing the atoms of a pure metal. The value of Q increases monotonically with an increase in the bond order. In other words, it can be seen that metals with a high bond order diffuse less easily. Accordingly, metals diffusing with difficulty are anticipated to have high structural stability at high temperatures and show promise as heat-resistant materials. In this sense, Nb- and Mo-based alloys are promising as ultra-high-heat-resistant alloys.

The most significant problem with these bcc metals is the lack of machinability at ordinary temperatures. For example, Cr-based alloys have better creep properties at high temperatures and oxidation resistance than Ni-based ones, but are not in widespread use as high-temperature materials because of the difficulties encountered in machining them. Figure 13 [not reproduced] shows the results of a three-point bending test of high-purity Cr metal.[18] Interestingly enough, when surface polishing was coarse, specimens underwent fracture with little plastic deformation, as shown in (a) to (c). It was the same when there was an oxide or nitride on the surface, as in (d). On the other hand, when the surface was finely polished or had undergone electrolytic abrasion, specimens deformed until they became U-shaped, as in (e) to (h). As in the above, Cr, like glass, is sensitive to surface flaws. Accordingly, the removal of this sensitivity to surface conditions is an important task for the future.

6. Intermetallic Compounds

It is well known that intermetallic compounds have been drawing attention lately as new ultra-high-heat-resistant materials. Figure 14 [not reproduced] shows the relationship between the softening temperatures of various materials and their melting temperatures in order to demonstrate the temperature extent to which they can be used.[19] Here, the softening temperature is defined as the temperature at which the strength of a material is 100 MPa (approximately 10 kg/mm^2). It is clear that Nb_3Al and $MoSb_2$ can be used up to higher temperatures than can silicon nitride Si_3N_4. However, all of these intermetallic compounds have a problem in that their ductility is poor at room temperature, as can be seen in ceramics.

In the case of intermetallic compounds in which the component atoms are arrayed regularly, in contrast to alloys, the atomic array is often disturbed by deformation. For example, a surface defect, called an anti-phase domain boundary (APB), is sometimes generated as a result of deformation. Needless to say, the thought is that a compound deforms more easily for lower amounts of APB energy. For example, it has been found by calculating the electronic structure that the APB energy of an NiAl compound with a B2-type structure is approximately 0.8 J/m^2.[20] This value is about 10 times larger than that of metals. As a reason for this, it may be pointed out that the interaction between Ni d-Al p is stronger than that of either Ni d-Ni d or Al p-Al p. Therefore, it is necessary to weaken the p-d coupling and lower the APB energy in order to enhance the deformability of the compound.

Recently, from a different viewpoint, the addition effect of an alloying element in TiAl of an L10-type structure is being investigated by molecular orbital calculations. As a result, it has been reported that the addition of an alloying element which decreases the p-d coupling and increases the d-d coupling in TiAl is effective for improving ductility.[21] It has also been pointed out from a study on the anisotropy of the elastic constant of TiAl by band calculations[22] that TiAl's brittleness is caused by the strongly directional p-d coupling. As in the above, it is believed from past studies that a reduction in the p-d coupling leads to improvement in ductility.

In addition, research has been conducted which simulates the electronic structure of the TiAl deformation process by means of molecular orbital calculations.[23] The results of calculations are shown in Figure 15 [not reproduced]. The ordinate is the bond order which shows the magnitude of the coupling between atoms above and below the slip surface. The abscissas, P_1, P_2 and P_3, correspond, respectively, to before, during and after deformation. From part (a) of the figure, it can be seen that the bond order during the intermediate stage (P_2) decreases slightly from the state before the deformation (P_1), returning to the magnitude of the initial state. The deformation process in which the old coupling is severed and a new coupling is generated is simulated. In parts (b) and (c), the bond order during and after the deformation is greatly reduced. A comparison of these results shows that the deformation to the ordinary dislocation direction (1/2[110], (111)), that will not disturb the crystal structure in part (a), is the easiest. On the other hand, it can be said that deformation in the direction which generates an APB in (b) or (c) or a complex stacking fault (CSF) is difficult because of a large decrease in the bond order. As in the above, in intermetallic compounds in which different kinds of atoms are arranged regularly, it is characteristic that the directional dependence of deformation is conspicuous.

As described above, it has become possible to discuss the mechanical properties of intermetallic compounds, which have so far been explained exclusively in terms of the dislocation theory, from the standpoint of electronic structures.

7. Conclusion

An alloy design method (d electron alloy design method) of heat-resistant metallic materials, centered around alloy theory, has been presented in this article.

It is possible to arrange experimental data and systematize it by using parameters representing the characteristics of the individual alloying elements as determined by the molecular orbital calculation method (DV-Xα cluster method).

It is believed that an accurate and less wasteful alloy development will become possible by combining the new design method and the conventional empirical rules. Moreover, ultimate design will become possible and the possibility of the development of high performance alloy materials is also high. Such design techniques are applicable not only to metallic materials, but also to ceramic materials. Toward the 21st century, a rosy unfolding of research on heat-resistant materials is anticipated.

References

(1) Sims, C.T., "Superalloys 1984," Gell, M., et al., ed., The Metallurgical Society of AIME, Warrendale, Pennsylvania, 1984, p 399.

(2) Boesch, W.J., Slaney, J.S., METAL PROGRESS, Vol 86, 1964 p 109.

(3) Woodyatt, L.R., Sims, C.T., Beattie, H.J. Jr., TRANS METALL SOC AIME, Vol 236, 1966 p 519.

(4) Morinaga, M., Yukawa, N., Adachi, H., IRON AND STEEL, Vol 71, 1985 p 1441.

(5) Morinaga, M., Yukawa, N., Adachi, H., J OF JPN SOCIETY OF METALS, Vol 23, 1984 p 911; Vol 27, 1988 p 165.

(6) Morinaga, M., Murata, S., Ezaki, H., J OF JPN SOCIETY OF METALS, Vol 31, 1992 p 599.

(7) Slater, J.C., "Quantum Theory of Molecules and Solids," Vol 4, McGraw- Hill, New York, 1974.

(8) Morinaga, M., Yukawa, N., "Computational Materials Science," Doyama, M., Yamamoto, R., ed., Kaibundo, 1987, p 152.

(9) Morinaga, M., "Basic Knowledge of Advanced Materials," Ohmsha, 1991, p 287.

(10) Morinaga, M., Yukawa, N., Adachi, H., J PHYS SOC JPN, Vol 53, 1984 p 653.

(11) Barrows, R.G., Newkirk, J.B., MET TRANS, Vol 3, 1972 p 2889.

(12) Morinaga, M., Yukawa, N., et al., PHIL MAG, Vol A51, 1985 pp 223, 247.

(13) Sims, C.T., J METALS, Vol 21, 1969 p 27.

(14) Matsugi, K., Murata, Y., et al., "Superalloys 1992," Antolovich, S.D., et al., ed., The Minerals, Metals & Materials Society, Warrendale, Pennsylvania, 1992 p 307.

(15) Yukawa, N., Morinaga, M., et al., "Reduced Activation Materials for Fusion Reactors," ASTM STP 1047, Klueh, R.E., et al., ed., American Society for Testing and Materials, Philadelphia, 1990, p 30.

(16) Matsugi, K., Yokoyama, R., et al., "Proc of the 4th International Conference on High Temperature Materials for Power Engineering 1990," Commission of the European Communities, 1990, p 1251.

(17) Morinaga, M., Murata, Y., Ezaki, H., "Proc of International Symposium on Materials Chemistry in Nuclear Environment," Tsukuba, 12-13 March 1992, p 241.

(18) Morinaga, et al., to be published.

(19) Saito and Morinaga, to be published. (20) Freeman, A.J., Hong, T., Xu, J.H., "Atomistic Simulation of Materials Conf," 1988, p 41.

(21) Morinaga, M., Saito, J., et al., ACTA METALL MATER, Vol 38, 1990 p 25.

(22) Fu, C.L., Yoo, M.H., PHIL MAG LETT, Vol 62, 1990 p 159.

(23) Saito, J., Morinaga, M., et al., "Proc of International Symposium on Intermetallic Compounds," 17-20 June 1991, Sendai, Japan Institute of Metals, 1991, p 105.

Properties of Heat-Resistant Alloys Mechanically Alloyed

936C1023E Tajimi CHO KO ON ZAIRYO SYMPOSIUM '92 in Japanese 3 Dec 92 pp 51-61

[Article by Susumu Isobe, Daido Steel Co.; English abstract provided by source]

[Text]

[Abstract]

Several oxide dispersion strengthened superalloys have been materialized through Inco's unique mechanical alloying. Some of them have recently proven to be able to withstand hostile environments up to 1350°C as skid rails in billet reheating furnaces. The MA [mechanical alloying] process also shows promise for use with exotic ODS [oxide dispersion strengthened] alloys, such as the intermetallic compound γ-TiAl with extremely high Nb.

1. Introduction

In heat engines, i.e., jet engines, rocket motors, etc., with the design operating temperature of their component members constantly being raised, high output and high efficiency have become increasingly advanced in recent years.[1] In particular, regarding the precipitation-reinforced- type Ni-based superalloys, which occupy the principal position in gas turbines, the manufacturing method shifted from forging to casting accompanying the increase in the volume fraction of the dispersed γ'-phase, and the cast product expanded from an equi-axed crystal to columnar crystal, and even these days to single crystals. As a result of these improvements, the operating temperature of superalloys was improved remarkably, although the limiting temperature of metals is believed to be around 1050°C. As a means of further increasing the operating temperature, oxide dispersion strengthening (ODS) is effective, and a special powder metallurgical technique for mechanical alloying (MA) has been developed as the corresponding manufacturing method.

In this article, we will present examples of new applications of the MA method to Ni- and Fe-based superalloys, as well as the experimental results of the trial application of this method to a heat-resistant intermetallic compound, i.e., high Nb-TiAl.

2. Ni- and Fe-Based MA/ODS Superalloys

2.1 Intraparticle Reinforcement by Particle-Dispersed Strengthening

As has been mentioned above, the dispersion-strengthened phase of Ni-based superalloys is the γ' [$Ni_3(Al,Ti)$] phase. It forms a complete solid solution with a matrix by solution annealing at high temperatures, produces a large amount of precipitate (with volume fraction of 65 percent in single crystal alloys) by the subsequent aging, and is characteristic in that it has excellent conformability with the matrix grid and does not tend to coagulate, becoming coarse. However, above 1,000°C, it becomes bulky by coagulation, and at still higher temperatures it forms a solid solution again with the matrix, losing the dispersed-strengthening function.

As such extremely stable dispersion phases, one may mention various kinds of oxides. Among them, the formation free energy of oxides of rare-earth and actinoid elements is far larger than that of the γ'-phase itself or of still more stable carbides. One oxide, i.e., thoria (ThO_2), which belongs to the latter group, had been used for thoria dispersion (TD)- Ni or TD-NiCr. However, since the handling of Th, which is an actinoid element, is difficult because of its α radioactivity, even if such radioactivity is weak, and the alloy powder which contains its oxide is manufactured by the dry-type coprecipitation method, it is not possible to deal with superalloys that include an active element, such as Al or Ti, and its use has thus been discontinued for a long time.

As a substitute dispersion phase for this, the Y oxide belonging to rare- earth elements, yttoria (Y_2O_3), was selected. INCO was developed as a technique for its dispersion, with the successful manufacturing method called mechanical alloying.[2]-[6] The raw materials used for blending are a pure metallic powder of the component element and fine Y_2O_3 particles, which are put in a ball mill filled with Ar gas. In the mill, the pure metal powder becomes thin flakes, and fine Y_2O_3 particles are captured on their bonding surfaces. The bonded powder aggregate in this state is sealed in a can made of soft steel, and is molded by hot extrusion sintering. During this process, the mutual diffusion between the layered flakes of pure metallic powder proceeds, the matrix becomes a completely uniform solid solution, and an alloy is obtained with a microstructure in which Y_2O_3 particles are finely dispersed in the solid solution. This is the reason that this method, by which an alloy is fabricated through a totally mechanical process using pure metal as the raw material and without going through a melting process, is called MA.

The dispersed phase Y_2O_3 has a secondary effect of markedly increasing the alloy's resistance to oxidation, similar to metallic Y, which makes the MA/ODS alloy useful.

Photograph 1 [not reproduced] shows a transmission electron micrograph of the structure of MA758 (described later) manufactured in this way.[7] The uniformly-dispersed phase is an oxide fine particle with a diameter of several dozen nanometers whose distribution scarcely changes, even after heating at ultrahigh temperatures of 1,350°C for 200 hours, proving that it provides an extremely stable strengthening phase.

2.2 Improvement of Creep Strength by Conversion to Unidirectional Bulky Particles

At high temperatures exceeding one-half of the melting point (in absolute temperature) of an alloy, the creep deformation of the grain boundary becomes dominant, and eventually grain boundary fracture takes place. The formation of columnar crystals by unidirectional solidification and single crystals in cast alloys of the type strengthened by precipitated γ'-phase was precisely to alleviate or remove the adverse effect of the grain boundary. A similar phenomenon also occurs in the grain boundary of alloys of the type strengthened by dispersed oxide. Accordingly, it is indispensable to provide a heat treatment which will generate a structure arrayed in one direction in obtaining bulky particles by secondary recrystallization. That is, in hot extrusion or in subsequent rolling, an aggregate structure by processing is developed as much as possible. Moreover, machining conditions are carefully set so as to leave the appropriate amount of strain energy which will become the driving force recrystallization.

In high-melting-point MA alloys, a unidirectional bulky particle structure can be obtained by simply letting them stand in a high-temperature furnace of above 1,300 to 1,3500°C. However, since an alloy with a matrix which has been strengthened by γ' precipitation, such as MA6000 (to be described later), has a low melting point of 1,327°C, it is not possible to apply high temperature annealing. Therefore, the zone annealing method, in which unidirectional recrystallization is made to take place under steep temperature gradient by passing it through a high frequency heating coil, is appropriate.

Photograph 2 [not reproduced] shows the corrosion macrostructure of the MA754 (described later) rod material subjected to high temperature annealing. The bulky crystal grain boundary is recognizable, and its aspect ratio exceeds 8.[6]

2.3 MA/ODS Superalloys of Inco Corporation

Currently, the only company which is making oxide-strengthened superalloys on a commercial basis is Inco Alloys International in the United States and Great Britain. The nominal chemical compositions [6] of major products and the solidus and liquidus temperatures measured by DTA[7] are shown in Table 1.

Table 1. Inco's Typical MA/ODS Superalloys[6],[7]

Alloy	Fe	Cr	Al	Ti	Y_2O_3	Ni	C	W	Mo	Ta	B	Zr	Solidus (K)	Liquidus (K)
Inconel MA754	1.0	20	0.3	0.5	0.6	bal	0.05						1685	1713
Inconel MA758	1.0	30	0.3	0.5	0.6	bal	0.05						1646	1672
Inconel MA6000	1.0	15	4.5	2.5	1.1	bal	0.05	4.0	2.0	2.0	0.01	0.15	1600	1633
Incoloy MA956	bal	20	4.5	0.5	0.5		0.5						1776	1794

The three kinds at the top of the table are Ni-based alloys of γ (so-called austenitic) structure. The first two alloys are made based on the conventional solid solution strengthened forged alloy Nimonic 75, with MA754 already being used in the stator vanes of military jet engines. A high-Cr version of this alloy, MA758, is recognized as being useful as a tool for molten glass.

The matrix composition of MA6000 is the same as that of the cast alloy IN738, and it is aimed at enhancing mid-temperature region strength through the strengthening of γ'-phase precipitation. It was employed recently in the stator vanes of turbines for private power generation.

The alloy MA956 is an Fe-based alloy with a ferrite structure. Its base is Fe-Cr-Al system FCH2, which is used as electric heating wire. Although this alloy is characterized by a melting point that is higher than that of Ni-based alloys and excels in oxidation resistance at high temperatures as well as resistance to sulfurization, since strengthening by precipitation does not work due to its nature as a ferrite system, it had not been treated before as a strengthened material. Oxide-dispersed strengthening by mechanical alloying changed FCH2 to an ultrahigh temperature strengthened material. By making active use of its characteristics, it is now being widely used for jigs in heat treatment (example exists of replacing Mo), flame revolving vanes for boiler burners, the fuel injection nozzles of diesel engines, etc.

In addition to the above, various kinds of new strengthened alloys of Y_2O_3 dispersion that have matrix compositions differing from those of conventional alloys have been developed.

In the mechanical alloying process, when treating raw material pure metallic powder, use has been made, since the old days, of a dry-type of vertical high energy ball mill (attritor) in which stirring by steel balls employing whirling arms was performed. The inner wall of this apparatus was covered with a water-cooled jacket to absorb the heat in the mill, preventing the raw material metallic powder from forming large lumps. Since an increase in the diameter of the mill markedly reduces the cooling effect, there are limits to how far its capacity can be augmented. For this reason, a very large conventional dry-type horizontal ball mill was developed as a facility for mass production, which has been operating for quite a long time. Photograph 3 [not reproduced] shows an example of such a mill which can process more than 1 ton of powder at a time.[6] The performance of the product made by using this facility is equal to or better than that of the product treated by the attritor, and the dispersion of properties within one lot or from one lot to another is extremely low.

2.4 Application to Skid Rails

Attaining high output and high efficiency are important subjects not only in the aerospace industry, but also in our iron and steel industry. One such example is the furnace for heating a billet for rolling, which is being operated these days at high temperatures of the 1,300°C level. In addition, in order to enhance the heating efficiency by removing the billet from the hearth, the conveyance mode has shifted from a walking hearth to a walking beam, and the height of the skid rails of the beams has the tendency to increase. Since the rails are constantly exposed to the high temperature atmosphere within the furnace, the fact that they reach a high temperature in the furnace must be taken into consideration. The rails lift very heavy billets in such a state, so the rail head recesses as a result of the creep deformation due to repetitious compressive stress. Moreover, since the mixture of oxidized scales of the billets and burned ashes that is deposited on the head is highly corrosive, the wear of the head due to corrosion cannot be neglected either.

Materials that were developed to withstand such a severe environment and have been used up to the present include various kinds of the Cr-Co-Ni-Fe-W system solid solution strengthened cast alloys. Composite type rails in which the head portion is thickened by an alloy layer containing large amounts of Cr carbide by means of plasma welding have been put to commercial use.[8] It should be mentioned that buttons made of ceramics, such as Si_3N_4 and SiC, were used on a trial basis since they had excellent ultrahigh temperature creep strength, but the conclusion was drawn that they could not be used unless some kind of coating were applied since wear by corrosion in the furnace atmosphere was unexpectedly high.

In the investigation for applying the MA/ODS superalloys to the rails, the data needed first was their ultrahigh temperature creep strength. Although data for estimating the strength up to 1,150°C had already been acquired, measurements beyond this temperature did not exist at all. For this reason, an ultrahigh temperature compressive creep test in the atmosphere was carried out for three commercial alloys, i.e., two kinds of Ni-based alloys, MA754 and MA758, and one kind of Fe-based alloy, MA956, excluding the low-melting-point MA6000 and using the conventional Cr-Co-Ni-Fe-W solid solution strengthened cast alloy as the comparison material. Setting the temperature range from 1,200 to 1,350°C and the longest time to 50 hours, the activation energy and stress index were obtained by analyzing the data for each alloy, and the compositional equation for a steady creep rate was derived.

Figure 1 [not reproduced] shows the creep strength under a compressive stress parallel to a unidirectionally-growing particle, the computation of which is based on the above-mentioned equation.[7] The strain rate is the usual valued referred to in rail design. Since, according to these results, all alloys maintain high strength at up to 1,350°C, design becomes possible for stress exceeding that of conventional alloys by more than 12 times.

The next requirement was to obtain corrosion data at high temperatures. In order to obtain the data, after a beaker test in which the sample was immersed in a synthetic corrosive medium, a long-endurance exposure test was performed by placing the coupon in a heavy oil-burning billet heating furnace of 0.16 percent S. Figure 2 [not reproduced] is the weight loss by corrosion of the coupon when it was exposed to an atmosphere of from 1,000 to 1,300°C for 2,050 hours.[7] According to these results, all three alloys demonstrate better corrosion resistance than the conventional material, and it was confirmed in particular that the wear of MA956 was extremely low.

Judging from the characteristics mentioned above regarding the suitability of MA/ODS superalloys for use in

skid rails, an application test in a furnace of the above-mentioned type was begun. In Figure 3, the hybrid structure of rails manufactured on a trial basis is shown.[9] Namely, only the head, which is exposed directly to the atmosphere in the furnace, is made of MA956, while the nozzle, which is placed over the water cooling pipe, is made of the conventional cast alloy. At 200 mm, the height from the top surface of the pipe to the upper end of the head is the greatest in the world.

Figure 4 [not reproduced] shows the recession of the head after it had been used for 7 months in an atmosphere of from 1,280 to 1,340°C/.[9] Although the rails for comparison are made of a composite which is said to be stronger than the conventional material, the wear of the MA956 head is less than one-third the recession of that material. Since it was possible to increase the height to 200 mm, the amount of heat inflow to the contact surface of the head and the billet was increased, and the width of the temperature drop of the so-called skid mark on the bottom surface of the hardened billet was decreased to one-half. In other words, what was 35°C for a height of 150 mm was decreased to 18°C in this case. The demonstration test of the skid rails made of high-performance MA956 will reach the 3-year mark in a few days.

Moreover, Ni-based MA754 and MA758 have demonstrated similar satisfactory results in several other billet heating furnaces.[7]

3. High Nb-TiAl Intermetallic Compounds Made by MA/ODS

3.1 Selection of Matrix Composition

For parts and body materials for the jet engines of supersonic transports and space planes, or for rocket motors, heat resistant alloys that are usable at metal temperatures exceeding 1,400°C are required.[1] Having already been put to practical use in the MA/ODS Ni- and Fe-based superalloys, the usable temperature is limited to around 1,350°C at the most. In order to obtain alloys that can withstand high temperatures beyond this temperature, it is considered necessary for high melting point metals to be adopted for the matrix.

High melting point metallic elements include Nb (melting point 2,467°C), Ta (2,996°C), Mo (2,622°C) and W (3,410°C). Since the strength of pure metals is low, various kinds of alloys aimed at dispersed strengthening by solid solution and carbide have been developed.[10] Although Nb has the lowest melting point of the above high melting point metals, since the density is low, i.e., 8.66 g/cm^3, it is considered to be appropriate as an aerospace material.

The greatest weakness common to high melting point metals is excessive oxidation at high temperatures and the resulting drop in strength. For this reason, a surface covering of silicide or aluminide is common, but its reliability is not high.

Although various improvements have been made to the oxidation resistance of Nb by adding an alloying element, there are many examples in which a large amount of Al is consumed due to the formation of an Al_2O_3 protective coating on the surface. The alloy with the best oxidation resistance among those reported is Nb-35/45Al-20/25Ti-4/6V-3/5Cr (numbers are at-percent).[11] In order to confirm these results and revise the Al content, four kinds of alloys of 100 g were manufactured by blending pure metallic powder and melting it in a button arc furnace. Figure 5 [not reproduced] shows the results of an oxidation test in a synthetic atmosphere at 1,200°C.[12] According to these results, the oxidation rate drops rapidly with an increase in Al content, with the rate constant for an alloy with an addition of 50 at-percent definitely lower than that with an addition of 75 at-percent of $NbAl_3$. Accordingly, the amount of Al added has been set at 50 percent higher than that in the above-mentioned alloy.

Such a high amount of Al and Ti far exceeds the solid solution limits of Nb. When this alloy is plotted in the Nb-Al-Ti ternary phase diagram at 1,200°C shown in Figure 6 [not reproduced],[13] it has a composition in which a single phase structure containing Nb at the solid solution limit in the intermetallic compound TiAl (γ, body-centered cubic system) of the Ti-Al system is formed, and this is confirmed by crystal structure analysis using X-ray diffraction. Since the Nb content is over 33 percent, which is the highest among the constituent elements (Al, which is next, is 30 percent) when the alloy composition is expressed in wt percent, it can be called a Nb alloy. However, the main body of this alloy is not the solid solution body of Nb (body-centered cubic system), but is the above-mentioned intermetallic compound.

DTA [differential thermal analysis] of this alloy showed that the change in the vicinity of 1,450 to 1,500°C (varies with the composition) of the binary system TiAl differs significantly from that expected for the melt reaction. Based on the fact that no indication was observable in heating to 1,650°C, the melting point is estimated to be higher than 1,650°C.

3.2 Manufacturing by Mechanical Alloying

Since there is a big gap between the melting points 2,467°C and 660°C of Nb and Al, respectively, that constitute this alloy, it is difficult to obtain uniform quality by melting. In the experiment using the button arc furnace, four melting repetitions were required, even though a pressure molded body of the mixed powder had been loaded. The blending of bulk raw materials is not considered feasible.

Mechanical alloying as a means of finely dispersing an oxide is thought to be appropriate as well for manufacturing alloy systems where melting is difficult. For this reason, a total of 3 kg of pure metallic powder and 0.6 wt percent of fine Y_2O_3 particles were loaded in a special dry-type horizontal ball mill, and were treated for 120 hours in a flowing Ar atmosphere. The compact extracted was sealed in a can made of soft steel to heat to 1,250°C, and was formed into a bar material with a diameter of about 17 mm under an extrusion ratio of 10. Photograph 4 [not reproduced] is a vertical section of macrocorrosion with the can intact, revealing that there are no cracks and that a homogeneous structure has been obtained.[14]

Photograph 5 [not reproduced] is the transmission electron micrograph structure of this material. The matrix is single phase and, according to the results of electron beam diffraction, is intermetallic compound TiAl of body- centered cubic crystal. Although the granular dispersed phase is an oxide, according to electron beam diffraction, it was not Y_2O_3 itself which was blended, but instead has been

identified as a compound oxide $Y_3Al_5O_{12}$ with Al_2O_3.[14] This is due to the progress of Al oxidation, although slight, during mechanical alloying, which is a phenomenon also observed in other alloys of high Al content. Since the grain size of the compound oxide is still small and its dispersion is uniform, its strengthening power is said to be precisely the same as that of Y_2O_3.

Figure 7 [not reproduced] shows the results of a long-term oxidation test at 1,350°C in the air (cooled to room temperature every 24 hours) of the MA/ODS material manufactured on a trial basis. Similar to the above-mentioned alloy employing the button arc furnace, the oxidation rate is low and no peeling occurs. Moreover, since a comparison with the oxidation rate of Inconel 600 (Ni-15.5Cr-8Fe), which, of the superalloys, exhibits excellent resistance to high temperature oxidation, at 1,100°C (the limits of this alloy's usable temperature) shows a low oxidation rate value of about two-fifths, it is judged that the oxidation resistance of this alloy is excellent.[14]

Photograph 6 [not reproduced] is the result of machining this hot extruded material as seen from the isothermal compressive test. The test piece is a compact one with a diameter of 8 mm and height of 12 mm, and it was set up to one-half of its height while maintaining the temperature through high frequency heating. From these results it can be seen that no cracks are generated, even for a high strain rate of 1.0 s^{-1} at temperatures as high as 1,300°C, thereby confirming that hot machining is relatively easy.[14]

The future tasks directed toward putting this alloy to commercial use are the setting of heat treatment conditions for obtaining the unidirectional bulky particle structure and the subsequent evaluation of ultrahigh temperature creep strength.

4. Conclusion

Using the mechanical alloying process to obtain alloys from pure metals without going through the melting process is most appropriate for manufacturing oxide-dispersion-strengthening-type alloys. The various kinds of Ni- and Fe-based superalloys being manufactured by Inco Corporation on a commercial basis have already been applied to the stator and rotor vanes of jet engines and gas turbines. However, it has been demonstrated that they are also useful for the skid rails of billet heating furnaces, and that they exhibit high performances as strength members, even at temperatures as high as 1,350°C.

This process will also be applicable to the manufacture of a high Nb-TiAl intermetallic compound, which is expected to be a material usable at still higher temperatures.

In the future, it is expected that the mechanical alloying technique will be applied to various alloy systems, and that new heat-resistant alloys other than those of the oxide-dispersed-strengthening-type will be developed.

References

(1) Tanaka, R., et al., "International Symposium on Ultra-High Temperature Materials '91," Tajimi, 1991.

(2) Benjamin, J.S., METALL TRANS, Vol 1, 1970 p 2943.

(3) Benjamin, J.S., Volin, T.E., METALL TRANS, Vol 5, 1974 p 1929.

(4) Benjamin, J.S., ed., "Frontiers of High Temperature Materials," Vol I, 1981, and Vol II, 1983, Inco.

(5) Weber, J.H., "Proc 25th Natl SAMPE," Azusa, California, 1980, p 752.

(6) Hack, G.A.J., ELECTRIC STEEL MAKING, Vol 57, 1986 p 341.

(7) Tsukuta, K., Iikubo, T., Isobe, S., "Structural Applications of Mechanical Alloying," in "Proc ASM Int Conf," 1990, p 99.

(8) Takagi, K., Hiraishi, H., et al., KAWASAKI STEEL TECHNICAL REPORTS, Vol 20 No 1, 1988 p 56.

(9) Tsukuta, K., Iikubo, T., et al., MATERIALS SCIENCE FORUM, Vol 88-90, 1992 p 229.

(10) "Handbook of Aerospace Engineering," edited by Aerospace Society of Japan, 2nd edition, Maruzen, 1992, p 191.

(11) Perkins, R.A., Meier, G.H., JOM, Vol 42 No 8, 1990 p 17.

(12) Tsukida, K., Iikubo, T., Isobe, S., DIGEST OF SPRING MEETING OF JAPAN SOCIETY OF METALS, April 1992 p 410.

(13) Perepezko, J.H., ISIJ INTERNATIONAL, Vol 31, 1991 p 1080.

(14) Tsukida, K., Iikubo, T., Isobe, S., DIGEST OR SPRING MEETING OF JAPAN SOCIETY OF METALS, Oct 1992 p 262.

On High Temperature Oxidation Phenomena of Inorganic Heat-Resistant Materials

936C1023F Tajimi CHO KO ON ZAIRYO SYMPOSIUM '92 in Japanese 3 Dec 92 pp 63-73

[Article by Toshio Yarii, Japan Ultra-High Temperature Materials Research Center; English abstract provided by source]

[Excerpt]

[Abstract]

In a high temperature oxidizing atmosphere, many materials oxidize and lose their original properties. Understanding the high temperature oxidation behavior of materials is important. Much research on the high temperature oxidation phenomena has been done on metallic materials. However, intermetallic compounds and ceramics are coming into use as high temperature materials. Moreover, in aerospace industries, C/C composites are the main candidate for use in space plane materials. In a carbon-based material, however, in contrast to its excellent thermal properties, oxidation occurs very easily. Therefore, it is essential that an effective oxidation protection system be developed. In this paper, some published data regarding the oxidation of these materials and an ultra-high temperature oxidation/sublimation testing machine located at the JUTEM Gifu Center will be introduced.

1. Introduction

When exposed to an oxidizing atmosphere at high temperatures, many materials form oxides and deteriorate, so it is important to understand the behavior of oxides at high

temperatures for materials that are used in such an environment. Although the study of the oxidation phenomena with respect to metallic materials has been carried out vigorously in the past, since the use of ceramic materials and intermetallic compounds as heat resistant materials is being considered, grasping oxidation characteristics is becoming important for these materials as well. In addition, the utilization of carbon/carbon composites is becoming indispensable in fields related to the aerospace industry. Since oxidation can occur easily in these materials that have carbon as the base material, the development of an effective protective system that will employ a material exhibiting oxidation resistance at the operating temperature and atmosphere to protect these materials is considered to be the most important task.

In this article, we will survey the basics of the oxidation phenomenon and confirm the degree of oxidation at high temperatures of heat-resistant materials based on the published data.

Moreover, the specifications and performance of the ultra-high temperature oxidation testing machine installed at this center will be presented, and items that will be of reference in evaluating the oxidation characteristics of heat-resistant materials at high temperatures will be described.

2. Oxidation Phenomena

Oxidation, in a wide sense, refers to reactions by which electrons are removed from molecules or compounds, or reactions by which combined hydrogens are deprived. In this article, however, we will simply consider the combination with oxygen as oxidation. It can be assumed that all of elements, except for inert gases, can combine with oxygen, i.e., can udergo oxidation, and oxides have been confirmed for each element. Taking Cr, which is a metallic element, as an example, many oxides can be generated, as shown in Table 1, depending upon the combination ratio with oxygen. However, many oxides become unstable under certain conditions, and the only one which can exist stably up to the high temperature range is Cr_2O_3.

Table 1. Cr Oxides

Oxide	Remarks
CrO	Unstable, Resolves to Cr & Cr_2O_3
Cr_2O_3	Melting point 2,300°C
CrO_2	Resolves to Cr_2O_3 at 300- 400°C
Cr_5O_{12}	Becomes CrO_2 above 200°C
Cr_2O_5	Becomes CrO_2 by heating
CrO_3	Melting point 196-200°C
CrO_5	Unstable, Resolves to CrO_2

Since the formation of oxides necessarily reduces the thickness of the substrate material and produces characteristics which differ from those of the substrate material, it is important to know how much oxidation is involved in maintaining strength. In particular, since, as a rule, the reaction rate is increased at high temperatures in chemical reactions, the consideration of oxidation is indispensable for materials that are to be used at high temperatures.

Let us assume that an atom of the base material, say, a metallic atom M, undergoes an oxidation reaction by being brought into contact with O_2 under certain conditions, forming an oxide material ($2M + O_2 = 2MO$). If the surface of the material is completely covered with this oxide and the oxide layer is compact, one might think that this material's contact with oxygen has been excluded. In reality, however, it is recognized that oxidation proceeds as the thickness of the oxide layer gradually increases.

In order for oxidation to proceed, it is necessary for the material element to move through the oxide layer to progress to the interface where oxygen is present, or for oxygen to move to the interface with the metal.

Since the oxide formed is essentially an ionic material, it is not possible to consider a neutral element moving through the reaction product, and for either a metallic element or oxygen it should be assumed that it will diffuse in the form of an ion with a defect in the material, such as a hole. However, while the Schottky and Frenkel defects applicable to stoichiometric ionic compounds permit the movement of ions, they cannot explain the material movement involved in the oxidation reaction since the movement mechanism of the electron is missing in them.

Therefore, for oxidation products, as is the case for many compounds, it will become necessary to take into consideration compounds of nonstoichiometric composition, i.e., those that can be regarded as semiconductors. By so doing, an electric charge can be assumed to be transported by the excess metal or oxygen deficiency for the n type, and by a metal deficiency or excess oxygen for the p type.

Under these conditions, one may assume the validity of the following simplified conditions:

(1) The oxide layer is a compact and completely adhered scale. (2) The movement of ions or electrons through the scale is a rate-determining process. (3) Thermodynamic equilibrium holds for both the metal/scale and scale/gas interfaces. (4) The thickness of the scale is larger than the distance at which the space charge effect is valid. (5) The solubility of oxygen in metal is negligible.

Under these conditions, it will be assumed that the rate of increase of the thickness of the oxide film is inversely proportional to the thickness of the film, i.e, $(dx)/(dt) = k/x$, where x is the thickness of the oxide scale and k is the rate constant.

Since the integration of the above equation gives $x^2 = 2kt$, this is called the parabolic rate rule. This is the theory by which Wagner established in the 1930's that the constant could be expressed in terms of the chemical potentials of the relevant chemical species, etc.

Even now, when the oxidation rate is measured, its conformity with the parabolic rule is examined to estimate the rate-determining process mentioned in (2) above.

If the conditions assumed by Wagner do not hold, the oxidation rate naturally deviates from the parabolic rule.

When the scale is very thin or the concentration of the oxidizing gas is low, or if there is a passage of oxygen gas in the scale, the rate-determining process becomes a reaction or absorption at the interface, with the reaction becoming what is called the linear rate rule in which oxidation

proceeds linearly. For example, in the oxidation of carbon materials, when the products are gases such as CO or CO_2, this rule is considered to be applicable.

In addition, as is found mainly in low temperature oxidation, the logarithmic rate rule is recognized in which the oxidation rate decreases due to an increase in the resistance of the diffusion path.

Ideally, a state in which the oxidation rate decreases according to the parabolic rate rule, for example, is expected. However, in oxidation under the actual environment, even sturdy scales are broken and rapid oxidation begins again, with oxidation proceeding through the repetition of scale regeneration and destruction.

Also often seen are cases in which such phenomena as the cracking and peeling of oxidized scales dominate the total oxidation rate. Such phenomena are catastrophic and should perhaps be handled by statistical techniques, but cannot be ignored in practice.

As sources of the generation of destruction of oxidized scales, one may consider the following:

(1) Volume changes of the oxide and substrate material. (2) Epitaxial stress. (3) Compositional changes in the substrate or oxide. (4) Point defect stress. (5) Oxide formation within the scale. (6) Recrystallization stress. (7) The shape of the test piece.

Even in an oxidation mechanism in which no stress is generated in the oxidized scale, if a cooling cycle is involved, then stress is generated due to the difference in the coefficients of thermal expansion of the substrate and oxide. In general, the coefficient of thermal expansion of the oxide is smaller, so a compressive stress is applied to the oxide during cooling.

The stress thus generated is released by the cracking or peeling of the oxide or by the plastic deformation of the base or oxide.

The separation between the base and the oxide might be thought to act to prevent the diffusion of the ions, stopping the progress of oxidation. However, the O_2 generation mechanism resulting from the release of the oxide becomes conceivable even if it does not depend on the inner diffusion of oxygen ions, and the progress of new oxidation in the spatial part can be assumed. Moreover, since the release itself means a decrease in the joined area between the scale and the base, leading to the falling of the scales, it would not be a desirable situation.

3. Oxidation Test Data

In the R&D projects involving advanced materials of ultrahigh resistance to the environment that employ the Agency for Industrial Science and Technology's next-generation system, research on heat-resistant materials, such as intermetallic compounds and carbon/carbon composites, are systematically in progress. Needless to say, material creation and formation methods, as well as strength evaluation, occupy the principal parts of the projects. At the same time, however, it is necessary to carry out research on resistance to oxidation when the usage environment is considered, and reports on this subject are gradually being made.

At this point, let us recall reports about the oxidation rate measured for various kinds of materials.

3.1 Intermetallic Compounds

High melting point metals, such as W and Mo, generally have poor resistance to oxidation and are oxidized quickly in the air at temperatures exceeding 650°C. Regarding Nb, its resistance to oxidation is improved by the addition of Al and the formation of the Al_2O_3 phase on the surface. Accordingly, in the Nb-Al intermetallic compound, an improvement of the oxidation resistance can be expected. As shown in Figure 1 [not reproduced], in order to form the Al_2O_3 phase necessary to obtain a sufficient resistance to oxidation, the addition of Al in an amount greater than that in the Nb_3Al composition is required. Figure 2 [not reproduced] shows the results of oxidation by the constant temperature rise of Nb_3Al powder using a thermobalance. It corresponds to the case of passing pure oxygen of normal pressure, indicating a weight increase due to oxidation beginning at around 400°C, and demonstrating a rapid weight increase due to ignition and combustion at approximately 800°C.

Regarding Ti-Al system intermetallic compounds, many results can be observed from the oxidation test.

First, the results of Ti-Al system weight changes due to oxidation as measured at various temperatures are shown in Figure 3 [not reproduced]. Below 873K, the formation of oxide film proceeds rapidly up to about 6 hours, although the amount of formation, at approximately 2 g/m^2, is small, while from that point to 48 hours, no growth is observed. Beginning at 1,073K, the weight gain proceeds at a relatively high rate.

According to ESCA [electron spectroscopy for chemical analysis] analysis, Al_2O_3 is formed in large amounts, and the formation of SiO_2 due to the Si contained in Al is also observed. In addition, TiO, TiO_2, Ti_2O_3, etc., are observed as well.

An example of the weight change in Ti-Al due to heating is shown in Figure 4 [not reproduced]. Many inflection points are seen in the weight curve. Al_2O_3 is formed up to the first inflection point, with TiO_2-rich film formed thereafter. After that, when the base becomes Al rich, Al_2O is formed again, and the oxidation rate is reduced by the protective action of this film. It is believed that a pattern is repeated in which, accompanying Al oxidation, columnar crystals of TiO_2 are grown in the vicinity of the interface, breaking the Al_2O_3 protective film, and the high oxidation rate status rises.

An example of TiAl oxidation in the atmosphere at 900°C is shown in Figure 5 [not reproduced].

By oxidation at 900°C for 100 hours, an oxide film of approximately 100 μm is grown that exhibits a multilayered structure. These layers are in the order of TiO, Al_2O_3, and TiO_2 + Al_2O_3, from the outside, with Al-deficient layers, such as Ti_2Al and Ti_3Al, formed on the substrate side as well. The process of oxidation progress is the formation of Al_2O_3 during the initial period, along with the formation of Ti_3Al in the substrate which becomes the supply source of Ti to the surface of the oxidized layer. It is believed that the diffusion of Ti in Al_2O_3 is fast, and that TiO_2 is formed on the surface of the oxidized layer.

In Figure 6 [not reproduced], the weight increase by oxidation for 96 hours in the air is plotted against the temperature. Although, at 700°C, the oxide is mainly Al_2O_3, whose oxidized scales are not easily peeled, the formation of TiO_2 becomes conspicuous above 900°C, with the oxidation rate becoming markedly greater.

The results of comparing the oxidation behavior of Ti and three kinds of Ti- Al intermetallic compounds are shown in Figure 7 [not reproduced]. The tendency for the degree of oxidation to decrease with the increase in the Al ratio is the same as in the case of the Nb-Al systems above.

That Al_3Ti shows excellent resistance to oxidation at 1,000°C can be seen in Figure 8 [not reproduced].

The weight change by oxidation for the case of adding a third element to TiAl is shown in Figures 9-12 [not reproduced].

The chemical compositions of the testing materials are shown in Table 2.

Table 2. Chemical Compositions of Test Samples

Sample/Component (in wt %)	Al	V	Mn	Nb	W	Si	Fe	Cu	B	O	Ti
TA (PSC)	34.9									0.066	Bal.
TAV (PSC)	35.2	2.12								0.121	Bal.
TAM (PSC)	34.1		2.25							0.121	Bal.
TAB (PSC)	35.3								0.05	0.046	Bal.
W1 (button)	35.5				0.06					0.065	Bal.
W2 (button)	34.8				0.5					0.101	Bal.
W3 (button)	35.6				4.72	0.02				0.046	Bal.
MW (button)	33.1		2.07		4.22	0.04				0.092	Bal.
N1 (button)	35.6			0.07						0.116	Bal.
N2 (button)	35.7			0.88						0.057	Bal.
N3 (button)	35.3			10.28			0.02	0.03		0.034	Bal.
NM (button)	32.0		2.09	10.74			0.01			0.087	Bal.

No improvement in oxidation resistance is observed in Mn.

Such an effect is observed in V, B, W and Nb, with a particularly large effect observable for an approximately 10 percent addition of Nb. The effect of Nb has also been confirmed in Ti_3Al.

Regarding Si, the effect is shown as indicated in Figure 13 [not reproduced]. In addition, it has been reported that there is a slight effect in Y and Hf as well.

3.2 Carbon-Based Materials

Concerning the carbon-based composites for which use at still higher temperatures is being contemplated, the development of an oxidation-resistant coating is indispensable since these materials essentially oxidize easily, and oxidation tests of these coatings are being carried out widely.

First, the results of oxidation tests are shown in Figures 14 and 15 [not reproduced]. In Figure 14 [not reproduced], for pitch-based and PAN-based high elasticity carbon fibers, a comparison is given among those carbon fibers whose surface sizing agent has been removed by MEK (methylethylketone) solution and those which have been further heated to 1,500°C in a vacuum to remove the oxygen-containing functional groups on the surface. The test was administered by taking 0.2 g of samples in quartz containers, passing air at 1 liter/minute, and by holding the sample for 2 hours per temperature. In the state in which the functional groups remain intact, the oxidation starting temperature is low and the weight reduction by oxidation is great.

Although the surface area to weight ratio differed since the diameter of the pitch-based fibers was slightly larger, the PAN-based fibers exhibited greater weight reductions.

Figure 15 [not reproduced] shows the weight reduction due to oxidation decreases with the application of a SiC coating. It is thought that the surface treatment of the fibers differed from that of the samples in the previous figure.

The weight changes for various carbon materials in the air when their temperature has been raised are shown in Figure 16 [not reproduced]. The rate of the temperature increase is 0.035 K/s. In the C/C composites, it is said that the weight reduction due to oxidation is greater than that of other carbon materials because the interface of the fiber and matrix becomes the activation point of the oxidation reaction.

Regarding C/C composites, the thought is that the matrix carbon has preferred oxidation, and thus the mixing of an oxidation resisting agent into the matrix carbon is being tried. For many compounds, up to 30 wt percent of an oxidation resisting agent is mixed, and after they are molded and sintered, the weight reduction has been examined by heating them in the air by TG up to 1,000°C. In compounds containing Si, SiC is formed during sintering, but its effect is not clearly observable. For compounds based on Mo, Ti, Zr and Cr, while the weight reduction decreases with the heat treatment temperature, this is more clearly observable in the three compounds shown in Figure 17 [not reproduced]. However, when the matrix carbon is assumed to be pitch-based carbon, it is taken into

consideration, in conjunction with the formation of a mesophase, that the only compound in which the oxidation resisting agent can be dispersed stably is ZrB_2.

Figure 18 [not reproduced] shows the results of oxidation tests for several kinds of C/C composites employing a thermal balance. For the PAN-based C/C composites, the initiation of oxidation is observed beginning at 550°C.

Since all of the carbon fibers, carbon matrices and C/C composites start oxidation in the range of 500 to 800°C, an oxidation-resistant coating becomes necessary. For the coating, glass sealing is generally applied to the SiC coating.

The reason for providing a carbide film and overlapping an oxide film is that oxide ceramics have large coefficients of thermal expansion, although they have excellent resistance to heat and oxidation, and can potentially react with the base material C/C composites at high temperatures, making it undesirable to apply them directly to the surface of the C/C composites. The use of SiC as the base film is due to the fact that SiC satisfies the requirement that the coefficient of thermal expansion be small and close to that of C/C composites, that it has heat resistance, does not react with C/C composites, and has good adhesiveness. The reason for sealing with a glass layer of SiO_2 or SiO_2 + B_2O_3 is that cracks are generated in the SiC layer. A sealing material is required to demonstrate good wettability to SiC and a low reactivity with C/C composites and SiC, and the above-mentioned sealing material is found to be effect in an atmospheric environment at 1,700°C. In addition, the SiC layer, too, is given a layered structure in which a diffusion layer lies beneath the CVD [chemical vapor deposition] SiC, as shown in Figure 19 [not reproduced].

The results of measuring the weight reduction due to oxidation by a burner with a flame temperature of 1,600°C for a C/C sample, a C/C sample coated with SiC through thermal decomposition CVD, and a sample further sealed with SiO_2 are shown in Figure 20 [not reproduced]. The effects of coating and crack sealing are clearly recognizable.

The results of measuring weight reduction due to oxidation by means of thermal balancing the coating systems, as shown in Figure 21 [not reproduced], are given in Figure 22 [not reproduced]. It has been found that Type I, i.e., the lamination of a CVD SiC layer and a conversion SiC layer with one less thick, is more effective. It should be noted that the weight reduction is thought to be due to the vaporization of the glass seal.

Figure 23 shows weight changes when C/C composites are exposed to the atmospheric environment for 30 minutes. The samples include four kinds, i.e., a diffusion-coated [DC] layer, a CVD SiC layer, and SiC sealed layers of the foregoing two layers, with the effect of the crack sealing being apparent and the difference between DC and CVD also observable. DC SiC is considered inferior to CVD SiC in compactness and purity. Because of this, it is believed that oxidation resistance can be ensured by laminating CVD SiC on DC SiC to form the base coating.

Figure 24 compares the results of several kinds of SiC coating methods, finding that the CVD of method A and a thickness of greater than 50 μm give excellent results. The kinds of SiC coating used here are described in Table 3.

Table 3. Kinds of SiC Coatings

Method A	CVD	C_3H_8, $SiCl_4$, H_2 at 1,100°C
Method B	CVD	Low deposition rate CVD
Method C	DCS	Change to SiC in SiO gas atmosphere
Method D	DCS	Change to SiC in SiC, SiO_2 powder
Method E	DCS	Change to SiC in Si, SiC, Al_2O_3 powder

CVD: chemical vapor deposition; DCS: diffusion coating system

In the foregoing, oxidation resistance performance has been examined for several materials, focused mainly on weight change. It has been found that, although their target temperatures differ, there is a marked difference between intermetallic compounds and C/C composites in the length of oxidation time and the rate of weight change due to oxidation. For the C/C composites, continued efforts toward exploring a high performance coating system that will fully exhibit the high temperature characteristics of the base material must be expended.

4. Summary of Oxidation Behavior of Intermetallic Compounds and C/C Composites

As described above, although active oxidation experiments on heat-resistant materials are being conducted, detailed analyses of the oxides formed are required in order to clarify the oxidation mechanism, etc. For application purposes, what is required will be the measurement of the oxidation rate, i.e., the measurement of the thickness of the oxidation scales and the measurement of weight change due to oxidation.

The oxidation resistance test of nonoxide fine ceramics is defined in JIS R 1609. It is a system in which, following the determination of weight change after holding a sample in a furnace in an atmosphere of 1,300 to 1,400°C for 100 hours, the change in bending strength is examined. Accordingly, since weight measurement is performed only before and after the test, many samples will be required in order to trace the weight change due to oxidation.

In addition to the above, use is made of thermogravimetric analysis. Although this method has an advantage in that the weight change during heating can be obtained on a continuous basis, there are limits to the temperature due to the heat-proofness of the sample chamber, etc., and the sample weight is limited to several grams. Because of this, the size of the sample is small, and when the weight change per unit area where oxidation reaction takes place is examined, there is a drawback in that calculation becomes impossible due to the thickness reduction of the object material.

A comparison of the data on the oxidation rate in the previous section shows that there are considerable differences in values, even for the same material name, and that there are various test methods. For bulk materials, a measurement of the oxidation rate something like the time change of weight/area is desirable, while for fibers, whiskers and particles, a display of the weight change/original weight cannot be dispelled. As in the above, regarding the oxidation test, the current stage is that of integrating the data obtained by various methods that are appropriate for the materials.

5. Extreme Ultrahigh Temperature Oxidation/Volatility Testing Machine

At the Japan Ultra-High Temperature Materials Research Center we have a facility which can measure the weight change due to oxidation of bulk heat- resistant materials on a continuous basis up to an unconventional ultrahigh temperature range. In the following we will introduce the facility and report on a portion of the oxidation characteristics of materials, as well as provide a performance evaluation of oxidation-preventing coatings.

The basic configuration of the device can be classified into heating system, temperature measurement system, atmospheric chamber, vacuum system, balance and analysis system, as shown in Figure 25.

(1) Heating System

Heating is done by means of a 30 kW xenon arc lamp. Light is condensed by an ellipsoidal mirror, and a sample placed in the vicinity of the ellipse's second focus is heated by the arc image focused there.

The ellipsoidal mirror is made of a metal, and is gold-plated in order to enhance the reflection efficiency. The mirror is a part of an ellipsoid of revolution formed by an ellipse with a major axis of around 900 mm and a minor axis of 700 mm. The electrode part of the lamp and the mirror are water-cooled.

The heating capacity of the lamp is as follows. Assuming the conversion factor to light of the input is approximately 50 percent, the mirror condensing factor is 0.8 and the transmission factor of the quartz dome is 0.85, a value of 310 W/cm^2 is obtained as the arc image part, 56 mm in diameter. With a reflectance of 0.8 for the sample surface, the heating factor is 250 W/cm^2, which corresponds to a temperature raising power of 2,600 K (approximately 2,300°C).

(2) Temperature Measurement System

The temperature of the sample surface is measured by a radiation thermometer of near infrared rays of 0.9 μm. This wavelength is included in the transmission wave band of the quartz dome used to adjust the testing atmosphere.

However, one cannot deny that the reliablity of the indicated temperature is spoiled by the fact that in the radiation thermometer, the reflected light from the lamp that has a wide band of emission wavelength is mixed in, as is the radiation from the high temperature sample, and that there are many cases in which the radiation factor of the sample at high temperatures is not known precisely.

(3) Atmospheric Chamber

The vacuum and analysis systems are enclosed in a quartz dome placed over a chamber made of stainless steel. For adjusting the test atmosphere, gas is introduced through a minute introduction valve, and a sample table in the dome is supported by an electronic balance. The inner capacity of the chamber is approximately 60 liters.

(4) Vacuum System

A turbo molecular pump and an oil rotary pump are used for evacuation to prevent contamination within the chamber, attaining a vacuum of the order of 10^{-6} Torr. Although a Knudsen-type ion gauge is used for the main measurement, (Varitron) and a Pirani gauges are also used.

(5) Balance

An electronic balance installed in the atmosphere adjusting chamber supports the sample table. Samples of up to 100 g can be placed over the sample table, and it can handle almost any material, provided that the sample is a plate-form of 30 mm square. This balance has a measurement sensitivity of up to 0.1 mg, and gas generating materials are excluded as much as possible in order not to interfere with the use in a vacuum environment.

(6) Analysis System

This device is capable not only of measuring changes in the sample weight due to heating in an oxidizing atmosphere, but also of analyzing the decomposed gases of the sample resulting from heating in a vacuum. The partial pressure of the discharged gases is measured by a quadrupole mass spectrometer. A mass spectrum chart up to the mass-charge ratio of M/Z = 200 can be obtained, and the change in the partial pressure can be displayed with the lapse of time for five principal kinds of gaseous components.

6. Conclusion

The high temperature oxidation of heat-resistant materials has been surveyed, focusing on the ideas established for metallic materials, and the oxidation test data have been examined for intermetallic compounds and carbon materials.

From now on, since the requirements for heat-resistant materials will become increasingly strict, not only will development in the manufacturing and processing aspects, but also research which can evaluate materials that match the requirements in the strength aspect, have to be advanced vigorously. At the same time, the importance of a heat-resistant performance evaluation that takes into consideration the use environment of the materials must naturally be emphasized. Under these circumstances, it will be our pleasure if the facilities at our center can be of use in the development and research of materials in various fields.

Development of Erosion Testing Machine As High Enthalpy Arc-Heated Wind Tunnel

936C1023G Tajimi CHO KO ON ZAIRYO SYMPOSIUM '92 in Japanese 3 Dec 92 pp 75-86

[Article by Kichinosuke Hanawa, Masahiro Ishii, Masashi Matsumoto, Ishikawajima-Harima Heavy Industries Co., Ltd.; English abstract provided by source]

[Excerpts]

[Abstract]

The current status of the plasma arc wind tunnel as an erosion testing machine is outlined. A plasma arc-heated wind tunnel of 20 kW was delivered in late November 1991 after the successful commissioning of various required testing. Additional testing was conducted mainly to assure the functioning of the Fabry-Perot interferometric spectrometer. This tunnel is now owned and operated as an erosion testing machine by the Japan Ultra-High Temperature Materials Research Center (JUTEM) Ltd. in

Tajimi, Japan. This apparatus may be useful in the erosion testing of advanced materials, such as composite and functionally-gradient materials, for the future hypersonic aircraft and space planes.

1. Introduction

From late in the 20th Century to the beginning of the 21st Century, innovative future generation aircraft, such as the SST/HST and space plane, are scheduled to be put into operation.

The technologies required for development cover a wide range of aerodynamics, thermodynamics, heat conduction engineering, materials, control, etc., and instead of the independent development of airplane bodies and propulsion systems, as has been the case in the past, an integrated system concept which takes mutual influences into account will become indispensable.

In materials development, the realization of lightweight heat-resistant materials is positioned as the key technology, and the R&D of various kinds of advanced composites, such as C/C composites, intermetallic compounds and functionally gradient materials has been advanced. In particular, regarding the horizontal take-off and landing type space plane, with the surface temperature of the airplane body at take-off and reentry reaching 1,800°C, its thermal environment is extremely severe. As for the propulsion system, the problem with heat is more serious than is the case for the body since it is accompanied by combustion within itself, reaching temperatures exceeding 2,500°C, necessarily requiring that lightweight materials that can withstand use at ultrahigh temperatures be found.

Characteristics that are required, although differing depending upon the structure and cooling system employed, may be considered as the following:

- Heat resistance (strength, rigidity, creep resistance, heat impact resistance, etc.)
- Oxidation resistance and corrosion resistance
- Resistance to space environment
- Machinability

In the development of the above-mentioned materials, along with the forming and machining technologies and nondestructive inspection technology, those materials permitting the structural design of the space plane and thermal protection/thermal management will be of high commercial utility.

Under these circumstances, in March 1991 we were asked by the Japan Ultra- High Temperature Materials Research Center, Inc. (JUTEM) to supply them with a wind tunnel that would satisfy the following specifications as a testing machine for investigating the erosion resistance characteristics at ultrahigh temperatures of the next-generation advanced materials:

Gas temperature	2,300°C
Gas flow velocity	not less than Mach 3
Gas type	nitrogen and air
Test duration	not less than 30 minutes
Specimen size	50 mm^2

The testing machine was delivered in November 1991 and was operated for demonstration purposes at the international symposium on ultrahigh temperature materials held during the same year.

Later, in March 1992, an additional test and the adjustment of a spectrophotometer for the measurement system were carried out to enable the real-time measurement of the gas temperature during testing, confirming that it was at the highest level in the world.

In this article, we will report briefly on the useful data obtained during the design stage, preliminary testing, manufacture, acceptance testing and additional testing.

2. Conceptual Design and Manufacture

Although the adoption of a diluted combustor which utilizes hydrogen combustion was also considered a candidate for the heater that is compatible with the gas temperature of 2,300°C, based on the judgment that the normal combustion time of the heater is several minutes at the most and that there are too many technological challenges, in order to ensure the required testing time of 30 minutes, we decided to employ a supersonic wind tunnel which uses an electric arc.

At Ishikawajima-Harima a 1-kW arc-heated wind tunnel for studying erosion characteristics resulting from the collision of atomic oxygen has been commercialized, and since the installation plans for a 20-kW arc-heated wind tunnel for space environment simulation were in progress, it was decided to advance the conceptual design through expansion and improvement by adding the functions of a supersonic wind tunnel.

As an existing facility of the same kind, a 450-kW arc-heated wind tunnel is in operation at the National Aerospace Laboratory, Agency of Science and Technology (NAL), but it was estimated that, of the above-mentioned specifications, it would be difficult to satisfy the requirements for gas temperature.[1]-[3],[5]

The conceptual design was advanced based on the in-house 20-kW arc-heated wind tunnel project by reflecting the results of the preliminary testing as much as possible.

(1) Raising the Gas Temperature

By employing the simple Huels-type electrode, similar to the 1-kW arc-heated wind tunnel, one assures reliability. In addition, the anode and nozzle are maintained at an equal potential to prevent drops in temperature from occurring during the expansion process of the gas.

(2) Gas Flow Velocity and Nozzle Diameter

Since the increase in flow velocity was not intended for the 1-kW wind tunnel and the gas flow was experiencing insufficient expansion, the area ratio was to be changed to secure adequate expansion for supersonic flow. In addition, the diameter of the outport was set to be increased to 100 mm to match the specimen size of 50 mm.

(3) Gas Flow

According to the plan for expansion from 1 kW, it will be 1.5 g/s, but by carrying out preliminary testing and emphasizing stability, the flow rate will be set in the range of from 1 to 1.5 g/s.

(4) Power Supply Capacity and Supply Facility

A 200 AX 150 V power supply was selected in order to satisfy the starting requirements of arc discharge and to ensure that there will be no problems for 20 kW rated operation.

Based on the above design concept, a design was advanced by deleting the plenum chamber provided between the anode and nozzle in the normal arc-heated wind tunnel (NASA and NAL), and preliminary tests were carried out, obtaining the following results.

(1) Gas Temperature By melting niobium, it was confirmed that the gas temperature was above its melting point (2,468°C).

(2) Heat Flux

By measuring the temperature rise of metallic copper, it was confirmed to be in the range of from 80 to 120 W/cm^2, so it was found that it could simulate the reentry of rockets and space planes into the atmosphere.

(3) Gas Flow Velocity

From the delamination distance of a shock wave in front of a cylinder, the gas flow velocity was measured at Mach 1.4 to 1.6.[5] On the other hand, from the total pressure ratio of the Pitot tube, a Mach number of 7.9 to 8.3 was calculated.[6],[7] Since the Pitot measurement presupposes an isentropic flow in front of and behind the shock wave, a different method of computation should be used in the present case where there is a heat supply source in the expansion process, leading to such a method being established.

(4) Gas Flow Rate

Since it was confirmed that the stability of the arc discharge was better for 1 g/s, it was decided to fix the flow rate at this value for the time being.

(5) Nozzle Material and Structure

As a result of a test in which copper was used without cooling, the temperature was below 240°C at every point during the test, so this one was adopted.

The design and manufacture was advanced by reflecting the above circumstances, with the manufacture completed in September 1991.

The on-site installation in the city of Tajimi, Gifu Prefecture, was completed in early October of the same year, experimental operation was carried out, and the apparatus was delivered at the end of November, as scheduled, after confirming that it had passed the required specifications. At that time, since the plasma temperature measurement employing the Fabry- Perot spectroscopic photometer was uncertain, an additional test was conducted in March 1992, and the apparatus was confirmed to be fully functional.

3. Summary of Facility

The facility system diagram is shown in Figure 5 [not reproduced]. The apparatus is installed in a room similar to the business office in the JUTEM building (see photograph in Figure 4 [not reproduced]).

The main body of the testing section is made of 304 stainless steel of 1 meter in diameter x 1 meter length, and during testing its interior is maintained at a degree of vacuum of 0.5 Torr or higher. In order to protect the apparatus from damage by thermal radiation of the plasma, its outside has a water-cooled jacket structure.

The arc-heating part is a Huels-type electrode, with the cathode made of thorium-tungsten and the anode made of oxygen-free copper, both having a water-cooled structure. The plasma generated by the arc is diluted by nitrogen or oxygen gas supplied through a separate passage, becoming a prescribed nitrogen plasma or an air plasma, and is led to the nozzle to form a high-speed gas flow.

The nozzle is made of copper and has a non-cooling structure. Since the nozzle is joined to the anode by a bolt, and thus has the same potential as that of the anode, it is designed to have an inflow of heat during the acceleration of the gas.

The specimen is mounted on a traverse device provided inside the main body of the testing section. The X and Y horizontal positions of the traverse device can be set during testing by a motor. The position in the height direction needs be set prior to the test, but this will not represent an inconvenience in practice since the test piece is normally exposed to the plasma at the height of the plasma center (see photograph in Figure 7 [not reproduced]).

Plasma gas that has passed the test piece is led to a water-cooled diffuser with a 600 mm diameter. Its outer periphery has a water-cooled structure, and in its interior six pieces of baffle board with cold water pipes are provided perpendicularly to the plasma flow to lower the gas temperature to the level necessary for the exhaust system.

The exhaust system consists of an 11-kW mechanical booster pump and a 22-kW rotary pump for exhaust in order to establish the vacuum level required. The pressure of the discharged gas is raised to atmospheric pressure by the rotary pump, and is discharged to the outdoors after having been sufficiently diluted by a ventilation fan provided in the laboratory.

Nitrogen, oxygen and argon (used for the starting arc) are stored outdoors, with the supply pipes laid in the underfloor pit.

The cooling water is supplied from the cold water tower installed on the roof of the two-story building, wiath the returned water supplied back to the cold water tower after being collected by the manifold.

The control and operation panel consists of an erosion testing machine control panel, a remote control panel, and a gas supply facility panel. Testing can be performed by controlling the vacuum of the test section, exhaust system and arc heating, and by setting a predetermined gas flow rate and the mixing ratio of nitrogen and oxygen by means of the above-mentioned panels. The remote control panel is placed close to the test section to facilitate manipulation by the operator. Other panels are installed on the wall side (see photograph in Figure 8 [not reproduced]). The remote control panel is equipped to permit the operator to operate the system by monitoring through a 300-mm-diameter observation window in the test section.

A 300-mm-diameter observation window is provided on either side of the test section, and the following items of measuring equipment have been installed.

(1) Gas temperature measurement: continuous measurement during testing by Fabry-Perot optical interferometer.

(2) Test piece temperature measurement: measured through the observation window by infrared thermometer, but care needs to be exercised with regard to directivity.

(3) Test piece surface observation: observed using high resolution CCD camera, making it possible to obtain hard copy by employing television or video equipment. Note that this cannot be used during temperature measurement.

(4) Gas flow velocity measurement: the total pressure is measured by a water-cooled Pitot tube device, and is converted. Note that this measurement cannot be made when a test piece is mounted, and that it must always be performed prior to a test.

All of the testing facilities have been installed in a laboratory with dimensions of 9 meters (length) x 6 meters (width) x 3.5 meters (height). The maintenance space is judged to be secure, if not sufficient.

4. Performance of Test Facilities

The specifications of the plasma power unit are given below, with a very stable plasma obtained partly due to fixing the flow rate at 1 g/s.

Current stability at voltage rise of 10%	within 0.7 s
Current stability at voltage fall of 10%	within 0.4 s
Stability at load variation of 150%	within 0.2 s

The required values for a plasma temperature of 2,300°C and a gas flow velocity of Mach 3 have been satisfied.

Since the noise value measured 1 meter from the apparatus was 60 dB(A), which is considerably lower than the required value of 80 dB(A), the sound insulation enclosure initially contemplated is not needed.

The vibration value was less than 0.03 G for the range of from 10 to 1,000 Hz, and it was judged that it does not influence the testing machines in the next room.

Regarding the gas temperature, although it was initially feared that 2,300°C could not be cleared, by the design concept of not providing a plenum chamber between the electrode (anode) and nozzle part, it was possible to obtain an unexpectedly high temperature. The results of temperature measurement of various kinds of plasma gases at various distances from the nozzle are shown below (also see Figure 10 [not reproduced]).

Table 3. Temperature of Plasma Gases (in K)

Type of Plasma	Distance from Nozzle (mm)		
	10	100	300
Nitrogen plasma	7,100	6,500	5,800
Air plasma	4,500	4,100	4,100

Thermal flux is the most important parameter when simulating reentry into the atmosphere and, again, results have been provided which are better than those of the preliminary testing (see Figure 11 [not reproduced]).

Table 4. Heat Flux of Plasma (in W/cm^2)

Type of Plasma	Distance from Nozzle (mm)		
	10	100	300
Nitrogen plasma	300	100	80
Air plasma	130	120	110

For determining the Mach number, measurement employing a Pitot tube was conducted. In contrast to the supply pressure on the upstream side P01 = 103 kPa, a Pitot tube total pressure P02 = 0.96 kPa was obtained. Therefore, as a result of computation by the use of the well-known expression that follows, a Mach number of M = 7.87 was produced.

$$\frac{P01}{P02} = \left(\frac{(k+1)M^2}{2}\right)^{\frac{k}{k-1}} \left(\frac{k+1}{2kM^2 - (k-1)}\right)^{\frac{1}{k-1}}$$

In the above, k is defined as the ratio of specific heats and is estimated to lie in the range of k = 1.1-1.3. The evaluation of the Mach number presupposes the presence of isentropic flow in front of and behind the shock wave, as mentioned earlier. However, this condition does not seem to be satisfied in reality, and this point will be discussed in the next section.

At any rate, we are convinced that a temperature higher than those obtained by NASA and NAL using similar arc-heated wind tunnels has been attained.

5. Evaluation of Design and Measurement Results

An important point in the design of the erosion testing machine is the fact that the plenum chamber between the electrode (anode) and the expansion nozzle has been eliminated, as mentioned earlier.

Since it has been reported that a wind tunnel can only secure a test-piece surface temperature of 1,400 to 1,700°C, the arc-heated wind tunnel at NAL in Japan was not used in view of our intention to minimize the heat dissipation at the plenum chamber of the high temperature plasma in order to achieve the required specification of 2,300°C.

Since results which far exceed the required 2,300°C have been obtained for the plasma temperature, we are convinced that we have demonstrated the validity of the design concept.

Regarding these results, although various discussions can be made, there are two reasons for them, i.e., a passive reason and a positive reason, based on the design concept.

The consideration from the passive point of view is the following. This is the fact that the gas flow rate has been reduced from the 1.5 g/s initially planned to 1 g/s in order to stabilize the plasma arc. In other words, the energy input from the arc to the unit gas flow has been relatively increased by 33 percent.

The positive reason is that by eliminating the plenum chamber, the heat dissipation is decreased and, relatively

speaking, the enthalpy of the plasma flow from the nozzle does not decrease. In addition, since the nozzle and anode are not insulated and are at the same potential level, it can be judged that the anode has expanded and the overall energy input can be considered to have increased.

The efficiency of an arc heater is said to be 30 to 50 percent, so 6-10 kW of the 20-kW capacity of the current erosion testing machine is expended to obtain the plasma gas. An arc discharge is established along a path through which an electric arc between the two electrodes can be formed easily. In the case of this machine, it is considered that a part of the arc discharge reaches as far as the nozzle since the nozzle is of the same potential as the anode. Assuming that both the flow expansion and heat inflow are taking place simultaneously in the nozzle, we will examine by computation a hypothesis to explain the difference between the Mach number 8 by Pitot tube measurement and the Mach number 1.6 by measuring the delamination distance of the shock wave.

Although it is not rigorous, we will examine the problem by dividing it into two processes. Namely, we will analyze the problem by assuming that the expansion process has been completed in a state in which no heat inflow exists, then when a heat inflow occurs in the plasma with a high Mach number.

Let us assume that the state in which air obtained by mixing nitrogen and oxygen is heated by an arc heater and is expanded isentropically by the nozzle can be represented as follows:

Total gas pressure	P01	100 kPa
Temperature of total gas	T01	2,500 K
Gas flow rate	W	1 g/s
Mach number	M1	8

The change in flow due to the heat inflow from this state can be analyzed and calculated by the method described in various textbooks.[6],[7]

$$Q = Cp * W * (T02 - T01)$$

$$\frac{T02}{T01} = \frac{M2^2 * (1 + k*M1^2)^2}{M1^2 * (1 + k*M2^2)^2} * \left(\frac{1 + \frac{k-1}{2}*M2^2}{1 + \frac{k-1}{2}*M1^2}\right)$$

$$\frac{P02}{P01} = \frac{P2}{P1} * \left(\frac{1 + \frac{k-1}{2}*M2^2}{1 + \frac{k-1}{2}*M1^2}\right)^{\frac{k}{k-1}}$$

where, Q is the amount of heat inflow (kW), T02 is the temperature of the gas following the heat inflow (K), P02 is the total gas pressure after heat inflow (kPa), P1 is the static gas pressure prior to heat inflow (kPa), P2 is the static gas pressure after heat inflow (kPa), and M2 is the Mach number following the heat inflow (-). In carrying out the calculations, the following quantities are assumed to remain constant:

Isopiestic specific heat of gas	Cp	1.15 kJ/kg x K
Ratio of specific heat	k	1.3

The results when the heat flow amount is changed can be obtained as follows:

Table 5. Flow Change Due to Heat Inflow

Amount of heat inflow Q (kW)	1	2	3
Mach number M2 (-)	3.10	2.09	1.50
Temperature of gas T02 (K)	3,370	4,240	5,110
Total gas pressure P02 (kPa)	1.10	0.40	0.27
Gas velocity V2 (m/s)	2,220	2,040	1,790

From the above calculations, if one assumes that, of the total amount of heat of 6-10 kW, approximately 2.5-3.5 kW is the heat inflow at the nozzle, it becomes possible to explain the discrepancy between the measured results of the Mach number by the two methods during the preliminary testing.

In this way it is judged that the initial design concept, i.e., the validity of the idea that the elimination of the plenum chamber will lead to an increase in the gas temperature, has been confirmed.

However, the drawback, i.e., that it becomes difficult to judge whether the dissociation of the plasma gas is in equilibrium, inequilibrium or a frozen state as a result of the elimination of the plenum chamber, remains unresolved.

From the international viewpoint as well, in testing facilities for simulating high enthalpy supersonic flow, e.g., in the free piston type impact wind tunnel, this problem involving gas dissociation, including a conversion method, is unresolved and remains to be solved in the future.

6. Evaluation of Plasma Gas

As shown in the previous section, by measuring the plasma gas temperature, useful data for setting the conditions for advanced materials testing have been obtained. Namely, for a plasma of 100 percent nitrogen and one of simulated air, quite different characteristics were obtained.

The nitrogen plasma exhibits gas temperature and heat flux values that are higher than those of air plasma, and is characterized by the distance from the nozzle being extremely sensitive. In addition, the scatter of the measured values is large, extending about 7 percent from the median value.

Air plasma exhibits gas temperature and heat flux which are about 30 percent lower. The change in the distance from the nozzle is flat and may be considered nearly

constant. The scatter of the measured values is small, ranging only about 2 percent from the median value.

That the stability of the plasma arc discharge is better in a nitrogen atmosphere is thought to be due to the inert property of the active atmospheric molecules in the oxygen-free state.

In spite of the above, we hesitate to recommend materials testing in nitrogen plasma. The reason for this is that, considering the circumstances that most of the advanced materials ordinarily developed are used in the aerospace field, as mentioned above, some doubt remains as to the validity of the test results in view of the difficulty encountered in converting the test data in nitrogen plasma to those in air.

Regarding the Fabry-Perot spectrophotometer, a measurement system has been established so as to enable measurement to be conducted after several adjustments have been made. From the fact that the useful results above were obtained by the Fabry-Perot apparatus, its importance is being recognized more than ever. This is because in a facility where gas is accompanied by luminosity, such as in an arc-heated wind tunnel or other high enthalpy wind tunnel, the tests themselves become meaningless unless the gas flow state is carefully confirmed.

7. Evaluation of Surface Temperature of Specimens

Although the temperature of the gas flow is important in determining test conditions, the most important parameter in test execution is the surface temperature of the specimen.

What one needs to pay attention to in an erosion test at high temperatures is to prepare, to the maximum extent possible, a specimen which does not require cooling, and to exercise care so as to not cause loss through heat dissipation.

The surface temperature of the specimens used in this arc-heated wind tunnel was estimated as follows.

The calculational model assumed that the heat inflow had been determined using heat flux data measured in advance, and that heat dissipation takes place only through thermal radiation corresponding to the emissivity of the specimen. For the emissivity of the specimen, data published on C/C composites, whose development is expected to be the highest, was used. However, in our calculations we ignored the effect of coating, which these materials usually have. The emissivities of the C/C composites are given below (taken from graphs in reference 11):

Surface Temperature (°C)	Emissivity
400	0.847
600	0.872
800	0.888
1,000	0.900
1,200	0.881
1,400	0.825
1,600	0.750
1,800	0.649

The calculational model is as follows:

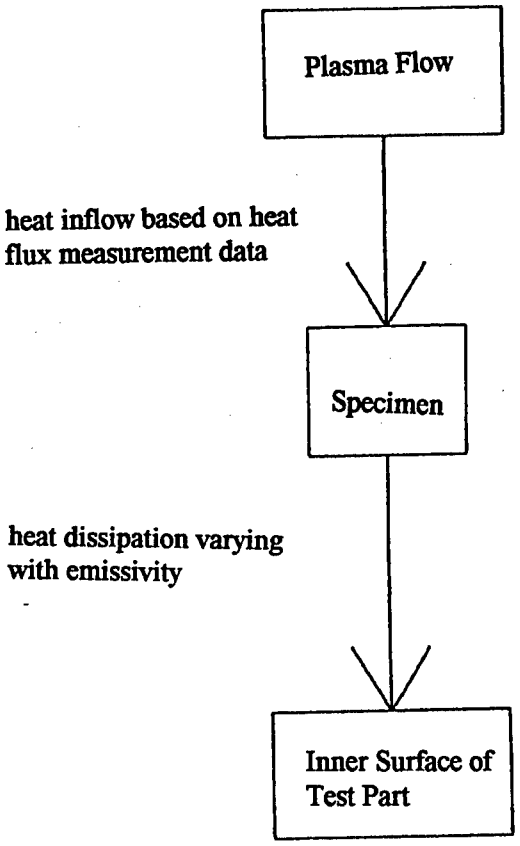

For air plasma, tests at extremely high temperatures are possible, and the results of calculations corresponding to this arc-heated wind tunnel are as follows:

At a position 50 mm from nozzle outlet	approx. 2,200°C
At a position 250 mm from nozzle outlet	approx. 1,700°C

Confirmation was carried out by making ceramic test specimens, and installing a thermocouple in the vicinity of the surface. The specimens were the following three types [Figure 13 [not reproduced]].

The confirmation test was carried out under the following conditions, the the measurement results shown in Figures 14 to 16 [not reproduced].

Applied power	18 kV (90%)
Gas flow rate	1 g/s
Component	nitrogen 80%, oxygen 20 %
Position	100 mm from nozzle

For simplicity, the specimen and holder were made in an integral manner, lacking heat-insulating material in the rear of the specimen, which happens in the actual case. Because of this, the entire unit is heated, and it takes

approximately 15 minutes to obtain stationary heat distribution. Therefore, although it differs from the actual case, it is believed that an overall evaluation is possible.

The results in an approximately stationary state after 20 minutes can be summarized as follows:

Table 6. Estimated Temperature of Specimens A, B and C

	Specimen A	Specimen B	Specimen C
Maximum indicated temperature (°C)	1,170	1,180	1,190
Estimated surface temperature (°C)	1,280	1,390	1,400
Heat flux in axial direction (kW/m^2)	35	28	34
Heat flux in radial direction (kW/m^2)	11	25	32

Since temperatures were obtained that were approximately 600°C lower than the values calculated for examination, some discussion is in order.

The aerodynamic heating at the stagnant point of the blunt hemispherical head object placed in an extreme supersonic flow, including dissociation, can be evaluated according to the following expression:

$$q = 0.763\sigma^{-0.6}(\rho\mu)^{(0.5)}(dU_e/dx)^{0.5}(hs\text{-}hw)\ \text{bracket}\ 1 + (Li^{0.52}\text{-}1)(ho/hs)\ \text{bracket}$$

$$dUe/dx = \text{Const.}*1/R\ \text{bracket}\ 2(Pe\text{-}P\infty)/\rho\ \text{bracket}^{0.5}$$

That is, it can be seen that it is approximately inversely proportional to the square root of the radius of curvature of the front edge.

In a separate measurement of heat flux, a copper pipe, 6 mm in diameter, was employed, and since a radius of curvature of 40 mm was used this time, its effects need to be examined. Also, by taking into account the fact that the applied power this time was 90 percent that of the previous time, the heat inflow q2 this time is estimated to vary with respect to the heat inflow q1 in the following way:

$$q2 = q1*(18/20)*(3/40)^{0.5} = 0.246*q1$$

In addition, since the dissipated heat which balances the heat inflow was almost entirely radiated during the previous test, w1 = q1. This time, since it is estimated that the heat dissipation due to heat conduction within the specimen is 10 to 20 percent, dissipated heat by radiation is set to be w2 = (0.8 to 0.9)*q2. Assuming that the emissivity of 0.6 to 0.8 is equivalent and obeys Stefan Boltzmann's law, the surface temperature T2 here may be considered to be given in terms of the temperature T1 = 2,200°C + 273 = 2,473 K, according to the following expression:

$T2 = T1*(w2/w1) = 2473*(0.246*0.8)^{0.25} = 1647\ K = 1374$ C.

In other words, it is believed that the validity of the current measurement results has been demonstrated.

However, since the fact that the surface temperature easily varies by more than 100°C, depending on the shape of the specimen, is clear from the current confirmation test of surface temperature, it may be said that the necessity for careful pre-testing examination has been confirmed.

In general, testing without pre-examining the specimen is not recommended, and one has to pay attention to the fact that it may give rise to insignificant test results or damage the specimen.

For the erosion test at 1,700°C, which has currently been suspended, it is believed appropriate to set the radius of curvature to 30 mm.

8. Planned Improvements for the Future

Although the required temperature of 2,300°C has been satisfied, one might say that it is too high a temperature.

Accordingly, instead of ensuring the stability of arc discharge in a state where the gas flow rate is virtually fixed at one point, as is the case currently, an improvement permitting operation over a wide flow rate range is desired. This is because the best situation for the testing machine is such that the test conditions of the erosion test can be set from a relatively low temperature to higher temperatures.

While the importance of the Fabry-Perot apparatus was mentioned in the previous section, measurement under the current conditions is possible only for a circular field of 30 to 50 mm. Under such conditions, neither a detailed study of temperature distribution within the plasma nor setting the position of the specimen other than the central part is possible. It is hoped that the apparatus can be improved such that the focal depth is changeable, thereby permitting finer tuning.

Concerning the infrared thermometer, its installation position was originally determined under the condition that measurement be taken for the specimen surface position not perpendicular to the gas flow, but rather inclined by 30°.[10] In actual testing, there have been many cases where a greater rise in surface temperature can be expected by placing the specimen perpendicular to the gas flow, and the directivity reduction of the emissivity has been conspicuous. Improvements matched with the actual situation are desired.[9] (see Figure 17 [not reproduced]).

A practical measure would be to change the location of the infrared thermometer which is now installed on a pipe on the outer periphery of the test section.

In the meantime, it is also recommended that a thermocouple, fully prepared for disconnection, be fixed in the interior of the specimen to obtain calibrated data.

Regarding the gas velocity, since it was not possible to measure it during testing, it remains unsatisfactory as test data. Rather than obtaining the relative Mach number by means of the Pitot tube, measuring the absolute velocity is by all means desired. There is a need to plan an absolute plasma velocity measurement by utilizing the effect of adding a measurement line to the Fabry-Perot thermometer or by adding another Fabry-Perot apparatus and utilizing the Doppler effect.

The dissociation of gas components of plasma is also an important parameter for evaluating the test results, and its

conversion corresponding to the portion in which the simulated dissociation differs from the actual situation in a high atmosphere is desired. Although such a method is currently under examination, the application of a copper vapor laser, induced fluorescence, etc., must be planned.

It is feared that the exhaust diffuser may not be recovering the kinetic energy of the plasma flow to static pressure with high efficiency. This is because the exhaust gas cooler is installed with its interior baffle plate perpendicular to the gas flow, and it is possible that its role as a baffle plate may be superfluous. When improvement of the gas velocity to higher than the current value is planned, a highly-efficient exhaust system which takes a self-ejector into consideration must be investigated.

9. Conclusion

An arc-heated high enthalpy wind tunnel, constructed as an erosion testing machine, has achieved a temperature higher than had been expected. It is desired that the design method employed from the beginning, i.e., the method of keeping the potentials of the anode and nozzle on its downstream side at the same level, etc., will contribute to the development of other projects. However, with the arc heater being an apparatus for which a design method has not yet been established, each unit has its own problems. Therefore, researchers are reminded that preliminary tests and verification are required every time a test is planned.

In addition, it is hoped that the improvement plan described in the previous section will be realized as soon as possible.

Moreover, with the capacity of this arc heater, at 20 kW, being extremely small, although it seems to be effective for the purpose of material development, its scale is too small and is not considered effective for testing under conditions approaching the actual situation faced by the future aerospace field. The size of the specimen is anticipated to be about 1 m x 1 m, an area which is approximately 400 times that of the present case.

Accordingly, the capacity naturally has to be increased by at least 400 times, and taking into account the degradation of the efficiency of the arc heater due to the gas flow rate accompanying an increase in size, an increase of 1,000 times is anticipated.

However, since this is considered to represent a test facility indispensable for the realization of products in the aerospace field, in particular, the space shuttle and space plane, we look forward to participating in a project that will utilize this experience at the stage when, at the earliest possible time, a plan for increased size comes up and a 10 to 100 MW project is realized.

In conclusion, we would like to express our thanks to the late Mr Ito, director, and Dr Yarii of Japan Ultra-High Temperature Materials Research Center, one of our customers, who provided us with cooperation, perseverance and appropriate comments on the road to project completion.

References (papers cited)

(1) Matsuzaki, T., Hirabayasi, N., et al., "The Characteristics of 450 kW Arc Heater," NAL TECHNICAL NOTE NO 545, April 1985.

(2) Aihara, Y., Nomura, S., "The Development of a Plasma Wind Tunnel," JOURNAL OF JAPAN AERONAUTICAL SCIENCE SOCIETY, Vol 12, No 122, January 1963.

(3) Hiraki, H., Aihara, Y., Nomura, S., "Experimental Studies Using a Plasma Wind Tunnel," JOURNAL OF JAPAN AERONAUTICAL SCIENCE SOCIETY, Vol 13 No 140, September 1965.

(4) Pope, A., Goin, K.L., "High Speed Wind Tunnel Testing," John Wiley & Sons, Inc.

(5) Thomas, S.R., Voland, R.T., Guy, R.W., "Test Flow Calibration Study of the Langley Arc-Heated Scram Jet Facility," AIAA-87-2165.

(6) Liepman, H.W., Roshko, A., "Elements of Gas Dynamics," John Wiley & Sons, 1957.

(7) Shapiro, A.H., "The Dynamics and Thermodynamics of Compressible Fluid Flow," The Ronaldo Press Co., 1953.

(8) Matsuzaki, T., Matsuzaki, R., et al., "Studies of Surface Heat Transfer in Arc-Heated Wind Tunnel," NAL TECHNICAL REPORT, TR-1048, December 1989.

(9) Heppenheimer, T.A., "The National Aerospace Plane," Pasha Market Intelligence, 1987.

(10) Siegel, R., Howell, J.R., "Thermal Radiation Heat Transfer," McGraw- Hill, 1972.

(11) Curry, D.W., Scott, H.C., Webster, C.M., "Material Characteristics of Space Shuttle Reinforced Carbon-Carbon," SAMPE, Vol 24, 1979 p 1524.

Reference Materials

(1) Hanawa, K., Tomioka, Y., Morimoto, S., "High Enthalpy Wind Tunnel for Erosion Testing of Advanced Materials," AIAA-92-3888.

(2) Morimoto, S., et al., "Arc-Heated Plasma Wind Tunnel—Completion and Testing," PAPERS ON 1992 THERMODYNAMICS SYMPOSIUM OF JSME, pp 81-82.